INITIATION OF INTERFACIAL TURBULENCE

IN LIQUID-LIQUID SYSTEMS

By

RICHARD DONALD SKINNER

Bachelor of Science
University of Arkansas
Fayetteville, Arkansas
1962

Master of Science
Oklahoma State University
Stillwater, Oklahoma
1964

Submitted to the faculty of the Graduate College
of the Oklahoma State University
in partial fulfillment of the requirements
for the degree of
DOCTOR OF PHILOSOPHY
July, 1967

INITIATION OF INTERFACIAL TURBULENCE

IN LIQUID-LIQUID SYSTEMS

Thesis Approved:

John B. West
Thesis Adviser

Kenneth J. Bell

C. Fremont Sams

K. C. Chao

N. D. Durham
Dean of the Graduate College

PREFACE

The phenomenon of interfacial turbulence has been used by investigators to explain the unpredicted high rates of solute transfer across some immiscible liquid-liquid interfaces. However, very little quantitative data have been observed relating to the causes of interfacial turbulence.

A review of the theories on interfacial turbulence reveals that a measure of the interfacial tension gradient along the immiscible liquid-liquid interface would aid in determining the conditions that would produce interfacial turbulence. Therefore, the objective of this study is to develop a method for measuring interfacial tension gradients along the immiscible interface and to determine the minimum gradient required to produce turbulence in several tributyl phosphate-n-heptane-uranyl nitrate-water systems.

I am sincerely grateful to Dr. J. B. West for his guidance and encouragement throughout this study. I am also thankful to Dr. R. N. Maddox for his help and encouragement while I was at the University.

I wish to thank Drs. B. D. Marsh, C. A. Sleicher, Jr., and W. J. Heideger of the University of Washington for the use of their computer program to determine the disturbance factors relating to interfacial turbulence in liquid-liquid systems.

Appreciation is also expressed to Mr. Calvin Slater for his suggestions and help with the experimental work, to Miss Amable Dorotan for her help in obtaining experimental data, to Mr. Eugene

McCroskey for his aid in the construction of the experimental apparatus, and to Mrs. Don Adams for typing this thesis. I thank my wife, Sandra, for her help and encouragement during my years in school at Oklahoma State University.

I wish to express my appreciation to the United States Atomic Energy Commission, under Contract AT(11-1)-846, for financial support during my graduate study.

TABLE OF CONTENTS

LIST OF TABLES

LIST OF FIGURES

CHAPTER I

INTRODUCTION

The transfer of a solute from one liquid phase to another is a frequently used process for the purification and separation of materials. Therefore, much experimental and theoretical research has been devoted to the study of rates of solute transfer between two immiscible liquid phases. The theoretical analyses which have been presented show good agreement with the experimentally observed rates of solute transfer for some systems. However, for some systems the rates of solute transfer predicted by the various theories are greatly different than the rates observed experimentally. Some investigators have attributed this difference to the existence of turbulence at the interface between the immiscible liquid phases (5, 20, 27).

The process of interfacial turbulence and spontaneous emulsification was first reported by Johannes Gad in 1878 (24). Since that time, several workers have investigated the causes and effects of interfacial turbulence when a solute is transferred between two immiscible fluids. These investigations have included a large variety of solutes and solvents. In liquid-liquid systems, most of the work has been conducted for the transfer between two immiscible liquids where one liquid is water (12, 15, 21, 28).

Interfacial turbulence is a phenomenon of physical motion at the interface of two immiscible fluids produced by internal forces between

the fluids. The term, "interfacial turbulence," defined by Sternling and Scriven (39), is any motion at the interface, ranging from a slight twitch to a violent agitation. There have been several theories presented predicting the causes of interfacial turbulence (7, 16, 17, 29, 34, 39), but none can be experimentally applied to explain every system for which interfacial turbulence is observed. Also, while several investigations of interfacial turbulence have been made, most investigators have presented only qualitative data related to the causes of interfacial turbulence.

The object of this work was: (1) to develop optical equipment for studying interfacial turbulence and (2) to obtain quantitative experimental data which could be related to the mechanism causing interfacial turbulence in liquid organic-aqueous systems.

A system of toluene-water-acetone was used in developing the methods for studying interfacial turbulence in immiscible liquid systems. A birefringent interferometer was constructed for measuring solute concentration gradients within the system. Also, modifications were made on a flowing junction cell in order that steep solute concentration gradients could be obtained along the immiscible liquid interface without causing interfering optical refraction patterns.

The systems used to study interfacial turbulence consisted of different concentrations of uranyl nitrate solute in organic (30 percent tributyl phosphate and 70 percent n-heptane)-aqueous solutions. The minimum step concentration differences of uranyl nitrate along the organic-aqueous interface required to cause interfacial turbulence were determined within ±0.02 molar concentration for all but one of the systems studied. The minimum step concentration difference

required to cause interfacial turbulence was determined for six different aqueous phase uranyl nitrate concentrations. The values for the step interfacial tension difference were obtained from a plot of interfacial tension versus aqueous phase uranyl nitrate concentration. The disturbance factors were calculated on a 7040 IBM computer using a modification of the computer program developed by Marsh, Sleicher, and Heideger (23).

CHAPTER II

LITERATURE REVIEW

Several attempts have been made by different investigators to explain transfer rates between liquids using variations of the film theory and the penetration theory. However, investigators have met with little success for some systems, using these approaches (36). Some investigators have attributed abnormally large mass transfer rates to interfacial turbulence (5, 14, 19, 20, 27, 42). Much work has been conducted studying different systems and conditions which produce interfacial turbulence, and some investigators have attempted theoretical explanations of the causes of interfacial turbulence (1, 7, 16, 17, 23, 26, 29, 30, 31, 32, 33, 34, 39). Sternling and Scriven (35) have presented a good discussion and literature survey of work (pertaining to interfacial turbulence) published from the beginning of interfacial turbulence studies in 1855 to 1960. Also, the theories relating to interfacial turbulence presented prior to 1966 have been summarized by Berg, Acrivos, and Boudart (9).

Interfacial Turbulence From Flat Film Studies

One of the early experimental investigations of interfacial turbulence was conducted by Bénard in 1900 (1). He was able to photograph the convection patterns of a thin layer of molten spermaceti resting on a metal plate heated to a uniform temperature, with a free

upper surface. Bénard observed that the most stable flow pattern was one of regular hexagonal cells and that a certain finite critical temperature gradient across the thickness of the layer had to be exceeded if any convection was to take place. Rayleigh, in 1916, attempted to explain the Bénard cells as being caused by convective instability due to an increase in density from the bottom to the top. Rayleigh's predicted critical temperature gradient was several orders of magnitude greater than that indicated by Bénard's experiments (1).

Langmuir and Langmuir (18), while studying the effects of monomolecular films on the surface tension of water, found that water saturated with ethyl ether burns actively when ignited, while a monomolecular layer of oleic acid over the solution extinguished the flame. They found that the rate of evaporation of ether from the covered solution was about nine times lower than that of the uncovered mixture. One explanation of the decrease in ether evaporation rate from the covered solution is that the molecules of ether are too large to penetrate the monomolecular layer of oleic acid.

Langmuir and Langmuir observed that a partially covered solution experienced twitching in the uncovered parts as long as evaporation was allowed to take place. They attributed the twitching to changes in interfacial tension along the surface. Along with this experiment and others, they were convinced that the decrease in evaporation of the ether was due to surface tension variations.

Block (2) noted that although Rayleigh's analysis failed to explain Bénard's observation, the analysis was in agreement with the experimental results of Schmidt and Milverton where both the top and bottom of the layer were bound by horizontal plates. Block extended

Schmidt and Milverton's work by producing Bénard cells on a thin layer of liquid. He was then able to extinguish the cells by covering the liquid with a monomolecular layer. The thickness of the liquid layer, covered by the monomolecular layer, was increased until Bénard cells were again observed. The thickness at which the Bénard cells were observed on the covered liquid was equal to the thickness calculated by Rayleigh's convection analysis. Block did further experiments in which he cooled the base plate on which the thin liquid layer rested and again observed Bénard cell formations. From the results of his experiments, Block stated that Bénard cells are caused by a different mechanism than convection and indicated that surface tension was the mechanism.

In Orell and Westwater's (28) studies of spontaneous interfacial cellular convection, about 30 systems were tested before a final selection was made. They chose the system of ethylene glycol-acetic acid-ethyl acetate because it produced a beautiful cellular pattern which lasted for days.

Orell and Westwater observed that, after the two unequilibrated liquid phases came into contact, the initial pattern on the interface underwent rapid changes before being stabilized into a typical cellular pattern. The cells were irregular shaped polygons ranging from three to seven or more sides and did not encompass the whole interface. There were, however, two basic types of cells formed: the stationary cells which were born, occupy almost fixed positions on the interface, tend to cluster along the test cell walls, and grow with time; and the propagating cells which were born, grow, travel about the interface, multiply by splitting, and finally vanish.

Although Orell and Westwater made the study by viewing the interface normal to its flat surface, by drawing an analogy to the Bénard cells, they assumed that the polygonal cells were caused by roll cells.

Gore (13) conducted his research along the lines of Orell and Westwater, using shadowgraphs to study Bénard cells and interfacial turbulence. He proposed that Bénard cells and interfacial turbulence are analogous, the difference being that Bénard cells develop at a vapor-liquid interface and are caused by temperature gradients, while interfacial turbulence develops at a liquid-liquid interface and is caused by concentration gradients. He observed that stationary, cellular flow patterns are to be expected to occur only in slightly unstable systems.

Interfacial Turbulence From Pendent Drop Studies

Lewis and Pratt (21), while attempting to measure the interfacial tension of unequilibrated liquids by the pendent drop method, noticed a pulsation of the drop which motivated them to make a further investigation of this phenomenon. They studied several systems allowing the solute to be transferred from the aqueous phase to the organic phase and from the organic phase to the aqueous phase for each system. In most systems studied, drop pulsation was observed for solute transfer from the organic phase to water whether the organic phase was the drop or the bulk phase. However, pulsations of the drop were observed only when uranyl nitrate solute was transferred from the aqueous phase to the organic phase. Lewis and Pratt noted that heat is absorbed when uranyl nitrate passes from an organic phase to water, whereas heat is evolved by the transfer of other solutes to water.

Therefore, they concluded that the pulsation of the drop was caused by the heat evolved in transfer. Their conclusion was strengthened by the fact that surface-active materials reduced the pulsation for every system. This reduced pulsation resulted from the surface-active materials decreasing the solute transfer rate and thus the rate of heat generation.

Garner, Nutt, and Mohtadi (12) continued Lewis and Pratt's work and observed differences in pulsating behavior and the type of motion within the drops. They concluded that the behavior and the type of motion within the drops depends on (1) rate of drop formation, (2) concentration of solute, and (3) nature of liquids. Garner, Nutt, and Mohtadi also allowed a steep concentration gradient to approach the organic-aqueous interface and observed that the drop would pulsate at that point. In addition, they observed that surface-active materials suppressed these phenomena.

Haydon (15) in 1955 investigated the kicking of a drop by squirting acetone up to a drop of water in toluene and up to a bubble of air in toluene. Both systems experienced kicking when the drop or bubble were formed in the pure toluene, but only the water drop kicked when the drop or bubble was formed in a uniform mixture of toluene and acetone. He found that it was possible to prevent kicking by adding proteins or detergents without preventing spontaneous emulsification. Therefore, Haydon concluded that spontaneous emulsification is not related to kicking but proceeds according to the mechanism proposed by McBain and Woo.

Haydon (16) later extended his study of pendent drop kicking in several systems, all of which contained one phase of water. He found

by adding sodium chloride to the acetone-toluene-water system that kicking was stopped; and, as the sodium chloride concentration was decreased, kicking was increased. He noted that while sodium chloride has practically no effect on the interfacial tension of the system, it does decrease the solubility of acetone in the water. Further, he observed that detergents inhibited kicking but did not alter the solubility of acetone in water. Also, Haydon found that while four (vol.) percent acetone in toluene lowered the interfacial tension of toluene-water appreciably, the acetone lowered the interfacial tension of toluene-detergent mixture very little. Therefore, he concluded that the interfacial tension changes occurring as a result of the heat of disassociation, proposed by Lewis and Pratt (21), were at most second-order effects since his experiments showed kicking when no appreciable diffusion could have occurred.

Interfacial Turbulence From Emulsification Studies

McBain and Woo (24) studied several systems in an attempt to explain the causes of emulsification. They concluded that spontaneous emulsification is partly due to local movements resulting from lowered surface tension. However, McBain and Woo feel that a more important factor in causing emulsification is the collision of molecules in diffusing columns. The collision of the diffusing solute molecules will drive solvent out of one phase into the immiscible phase. They also found that soap is not an emulsifier but is merely a stabilizing or protective agent for droplets that have been formed by some other means.

Mansfield (22) in extending McBain and Woo's work concluded that

spontaneous emulsification is more a function of the change in interfacial tension than in the actual interfacial tension of the system. However, Mansfield does not agree with Stackelburg, Klockner, and Mohrhauer's assumption that spontaneous emulsification results from a negative interfacial tension.

Interfacial Turbulence From Liquid-Liquid Mass Transfer Studies

Ward and Brooks (43) in their study of free diffusion of acetic, propionic, n-butyric, and valeric acid across a toluene-water interface, found that while the transfer of acetic and propionic acids agreed with their theoretical calculations, the transfer of n-butyric and valeric acid gave anomalous results. They attributed the anomalous results to interfacial turbulence.

Hahn (14) found that the transfer of uranium across the interface followed the theoretical value more closely when surface-active agents were present. He observed that by adding 100 ppm of sorbitan monoleate to the aqueous phase, the transfer rate was decreased. Hahn concluded that the function of the surfactant is to block off the approach of uranyl ions to the interface, thereby suppressing the energy of reaction and the resulting convection.

Lewis (19) studied the transfer of solute between two immiscible liquids where the liquids were stirred in each phase. Lewis found that adsorbed interfacial films of the mobile type had no effect on transfer, while rigid protein films caused a retardation to transfer which he concluded was probably due to dampening of interfacial turbulence. Later in his study of the transfer of uranyl nitrate between

an organic and aqueous phase, Lewis (20) found that the observed solute transfer rates were higher for some systems than were predicted theoretically. For each of the systems experiencing high transfer rates, he observed interfacial turbulence at the interface.

Burger (5) observed that surfactant molecules reduce the transfer rate in either direction of uranyl nitrate in TBP-aqueous systems. He stated that the reduced transfer rate was probably due to mechanical blocking at the interface, although some effect may occur from preferentially replacing TBP at the interface. Also, he stated that interfacial turbulence occurred during uranyl nitrate transfer in some of the systems studied.

Bush (6), in measuring mass transfer rates of uranyl nitrate between an aqueous phase and an organic phase of TBP-Amsco, observed a more rapid transfer than was predicted by the individual film correlations reported in the literature. Although Bush never mentioned observing interfacial turbulence, in order to determine if interfacial turbulence could exist in his system, he applied Sternling and Scriven's theory. Bush concluded that interfacial turbulence does not occur in the transfer of uranyl nitrate across the water-TBP interface since interfacial tension increases with uranyl nitrate concentration. However, he did recommend the measurement of interfacial tension of the uranyl nitrate-water-TBP system at non-equilibrium conditions in order to further evaluate the possible existence of interfacial turbulence.

Theory of Interfacial Turbulence Caused by Density Gradients

One of the first theoretical explanations of interfacial

turbulence was presented by Rayleigh in 1916 and was based on the assumption that convection currents caused by a density gradient were responsible (30). Rayleigh was attempting to explain the results of Bénard's work by calculating the minimum liquid thickness that would be unstable for a given temperature gradient across the liquid layer. However, Rayleigh's theory predicted a minimum thickness which was an order of magnitude greater than that observed by Bénard (2).

Jeffreys (17) later extended Rayleigh's work by applying a more realistic set of boundary conditions. Rayleigh's solution applied to a fluid with a free surface at both top and bottom and with the temperature maintained constant over both. Jeffreys presented solutions for each of these cases in which he determined the minimum Rayleigh number,

$$R = - \frac{g \gamma \delta h}{K \nu} ,$$

required to give an instability for the system.

Pellew and Southwell (30) presented a much more detailed derivation of fluid instability caused by a temperature gradient than did Jeffreys. They also attempted to show mathematically that the hexagonal Bénard cell is the most stable pattern formed.

Sani (32) recently studied the stability of an infinite horizontal thin liquid layer to buoyancy-driven finite amplitude roll cell disturbances. He developed equations to predict what systems could have stationary and oscillatory instabilities. The parameters used by Sani to determine if the system will be stable or will experience stationary or oscillatory instabilities are the mass Rayleigh number, the ratio of the Prandtl number to the Schmidt number, and the second and third coefficients of the amplitude equation.

Theory of Interfacial Turbulence Caused by Interfacial Tension Gradients

Haydon (16), assuming that the kicking of a drop is caused by interfacial tension changes, derived an expression for the mechanical energy acquired by the drop for a change in interfacial tension over a small part of the surface. Davies and Haydon (7) then calculated from the dynamics of the oscillation the energy dissipated by the drop. They were able to make a time-displacement plot of the drop by photographing the oscillation of the drop at 64 frames per second. The kicking of the drop was artificially stimulated by squirting a small amount of solute to the center of the drop and at a right angle to the camera. Davies and Haydon felt that the calculations of the energy acquired by surface tension changes agreed with the calculation of the energy dissipated by the drop within experimental error. Therefore, they concluded that their theory for the cause of the drop kick was correct, since the energy acquired was calculated from interfacial tension changes and the energy dissipated was found independently of the interfacial tension changes.

Pearson (29) has proposed a mechanism in which the cellular convection motion observed by Bénard can be induced by surface tension forces. The explanations of Bénard's observations have hitherto been attributed to the action of buoyancy forces. Pearson used an approach similar to that used by Jeffreys but applied a term for the surface tension variation with temperature. From this approach Pearson derived another dimensionless number,

$$M = \frac{\sigma \delta h^2}{\rho \nu K},$$

(Marangoni number) which corresponds to the Rayleigh number. Pearson found, by comparing the Rayleigh number obtained by Jeffreys (17) to his Marangoni number, that surface tension variations for most liquids at laboratory temperatures would be predominant in causing convection currents in liquid layers less than one cm. thick. He pointed out that his theory was in much better agreement with Bénard's experiments than those theories based on buoyancy forces.

Sternling and Scriven (39) have analyzed a simplified mathematical model in order to detail the mechanism of the interfacial engine. Although their model is too simplified to be reproduced in the laboratory, they have obtained much qualitative information from their study. Their analysis suggests that interfacial turbulence is usually promoted by

> (1) solute transfer out of the phase of high viscosity, (2) solute transfer out of the phase in which its diffusivity is lower, (3) large differences in kinematic viscosity and solute diffusivity between the two phases, (4) steep concentration gradients near the interface, (5) interfacial tension highly sensitive to solute concentration, (6) low viscosities and diffusivities in both phases, (7) absence of surface active agents, and (8) interfaces of large extent [39, p. 514].

Sternling and Scriven (39) have also presented a qualitative explanation of the roll cell. A very brief summary of their explanation is presented with the aid of Figure 1.

If a solute is being transferred from phase A, which has a higher viscosity and lower diffusivity, to phase B, roll cells of the type shown in Figure 1 will be reinforced if the interfacial tension for the two phases decreases with an increase in solute concentration.

> The interface is no longer in mechanical equilibrium and seeks a state of lower free energy through expansion of regions of low interfacial tension at the expense

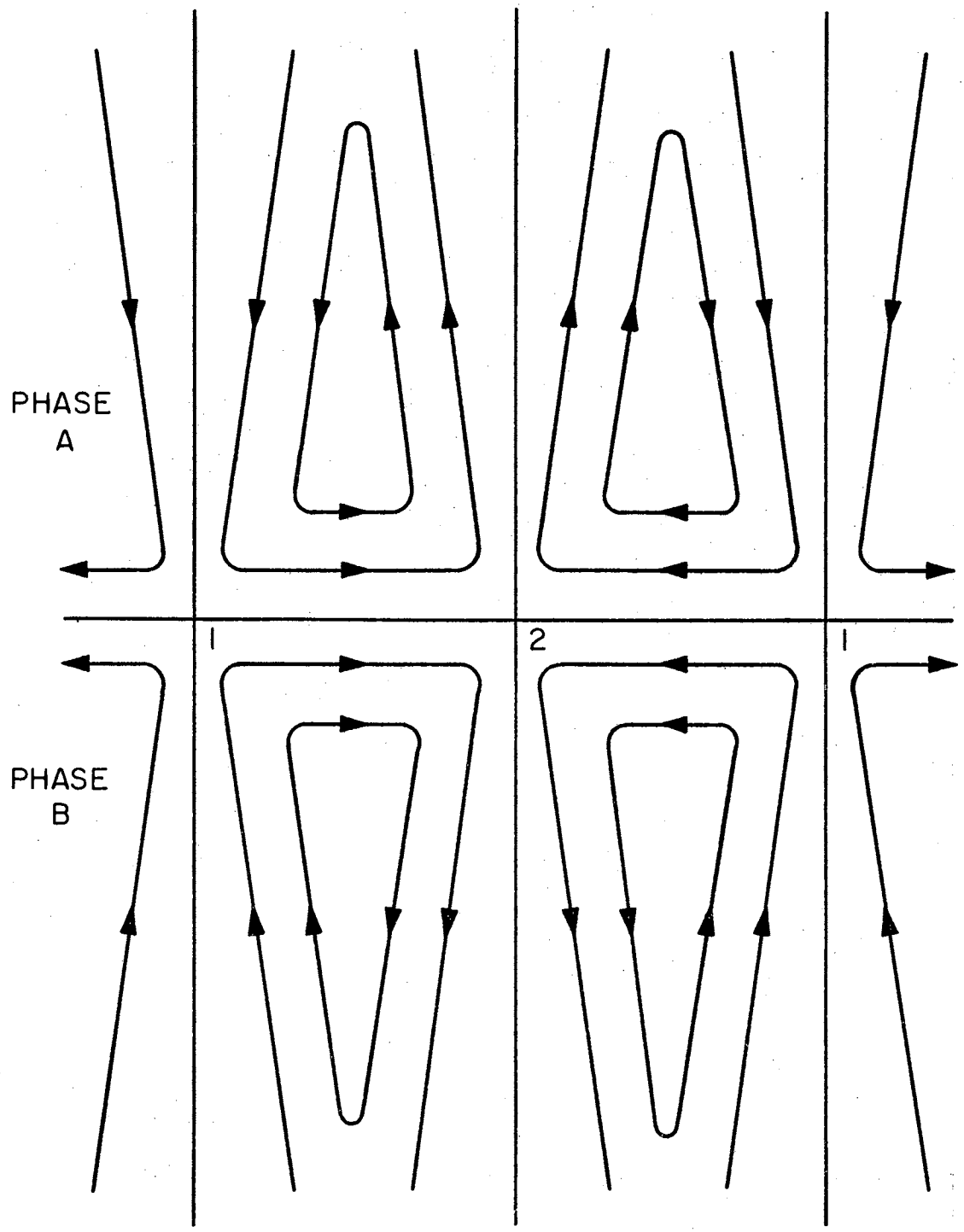

Figure 1. Two-Dimensional Roll Cell Model

> of adjacent regions of higher tension (the Marangoni effect) [39, p. 516].

The roll cells will be damped if the interfacial tension is increased with increased solute concentration, because the Marangoni effect will impose a flow opposite to the direction of flow of the roll cell. However, the reverse is true if the same solute is transferred from phase B to phase A. This led Sternling and Scriven to the remarkable conclusion that the system they studied is always unstable relative to roll-cell disturbances, if not with solute transfer from phase A to phase B, then with transfer in the opposite direction. Scriven (33) has extended this work by deriving a completely general formulation of the dynamics of a Newtonian fluid interface.

Marsh, Sleicher, and Heideger (23) have extended Sternling and Scriven's work. They have duplicated the roll-cell model with slight modifications to show that both stationary and oscillatory instability can exist. Their explanation of oscillatory instability is that it is caused by overstability. Overstability occurs when the ratio D_A/D_B is much greater than one, for transfer from phase A to phase B. When D_A is much greater than D_B, the undisturbed concentration profile in phase A is restored by molecular diffusion more rapidly than the undisturbed concentration profile in phase B. Therefore, the system for which the interfacial tension decreases with an increase in solute concentration experiences an interfacial tension force along the interface that opposes the motion of the original disturbance. The original motion of the roll cell is, therefore, reversed repeatedly.

Marsh, Sleicher, and Heideger's model was based on the roll cell model used by Sternling and Scriven with the following assumptions:

> The interfacial tension is assumed to be large enough

> so that the interface will remain flat. The two phases are in thermal equilibrium, and the interface is assumed to be in thermodynamic equilibrium at all points of contact [23, p. 8].

Marsh, Sleicher, and Heideger have derived an equation for a dimensionless growth constant, B, assuming the actual growth constant, β, is not equal to zero. They introduced the following form of the stream function, ψ:

$$\psi = \phi\,(x)\; e^{i\alpha y}\; e^{\beta t}$$

where α is the wave number and β, a complex number, is the actual growth constant. Using the flow, continuity, and diffusion equations, they derived the following expression:

$$B = \frac{\mu_a}{C_o\,\zeta_a\,\alpha}\,\beta = \frac{\frac{2}{\sqrt{\pi}}\,m\,\left\{\frac{q_b - 1}{q_b - p_b}\,\frac{1}{r} - \frac{q_a - 1}{q_a - p_a}\right\}}{\left[(1 - p_a) + \frac{\mu_b}{\mu_a}\,(1 + p_a) + \frac{\alpha\,\mu_s}{\mu_a}\right]\,\left(\frac{m}{r^2}\,q_b + q_a\right)\,(r + m)} \qquad (1)$$

Those disturbances for which the real value of the growth constant is negative are damped, and those with positive real growth constants are amplified and are said to be unstable either to stationary or to oscillatory instability.

> The dominant disturbance is that cell size which is amplified the most rapidly, i.e., has the highest value β for any given set of physical parameters [23, p. 22].

Marsh, Sleicher, and Heideger solved Equation 1 on the IBM 7094 digital computer for several sets of physical parameters. They have plotted their results with the real value of the growth constant or disturbance factor, $\hat{\beta}_o$, versus the ratio of the diffusivity of phase A to the diffusivity of phase B, r^2, and with $\hat{\beta}_o$ versus the

concentration distribution coefficient, m. In these plots, parameters of constant values were assumed for D_A, m, e^2, r^2, and ν_A. From this study, they predicted stability for liquid-liquid systems only when the solute diffusivities of the two phases are nearly equal (i.e., $0.95 \leq D_A/D_B \leq 1.05$). They also predicted that all other cases are unstable to stationary instability for solute transfer out of the phase of lower diffusivity and to oscillatory instability for solute transfer out of the phase of higher diffusivity. This explanation applies to systems for which the interfacial tension decreases with increased solute concentration. However, the reverse is true for systems in which the interfacial tension increases with increased solute concentration.

Berg and Acrivos (1) have extended Pearson's work by adding surface viscosity to the viscous term and letting surface tension be a function of both temperature and surfactant concentration. They found that a gaseous monolayer of surfactant (1/100 the number in a close packed film) would increase the Pearson number by seven orders of magnitude. This would indicate that for an interface covered by a gaseous layer of surfactants a temperature gradient of about 180°/cm. would be required for instability; and, for a condensed film, instability would be impossible by surface tension variations. They also pointed out that surface viscosity is relatively unimportant as a stabilizer when compared with the surface elastic effect.

Rukenshtein (31) has presented a paper where he includes the Marangoni effect in computing mass transfer rates from two phase liquid films in laminar flow. The equation derived for mass transfer includes the term, $\partial\sigma/\partial z$, interfacial tension gradient along the interface, which can be either positive or negative. If $\partial\sigma/\partial z$ is

positive, the rate of mass transfer is increased by the Marangoni effect; and, if it is negative, the rate is decreased.

Theory of Interfacial Turbulence Caused by Combined Effects of Density and Interfacial Tension Gradients

Scriven and Sternling (34) have extended Pearson's stability analysis by accounting for the possibility of sharp deformations of the free surface. They found that there is no critical Marangoni number for the onset of stationary instability and that the limiting case of zero wave number is always unstable. The assumption that the free surface is perfectly flat was found to confer on the liquid layer greater stability at large wave lengths than existed when the interface deforms elastically.

Scriven and Sternling also found a simple criterion for distinguishing visually the dominant force, buoyancy or surface tension, causing cellular convection in liquid pools. They showed that in steady cellular convection driven by surface tension, there is upflow beneath depressions and downflow beneath elevations of the free surface. They point out that for buoyancy driven flows the converse is true. Therefore, they conclude from Bénard's words and illustrations that the steady flows Bénard saw were all driven by surface tension.

Nield (26) combined the terms of buoyancy, explained by Rayleigh, and the terms of surface tension, explained by Pearson, in deriving equations to explain Bénard's observations. He found that the two agencies of instability reinforce one another and are tightly coupled. The cells formed by surface tension are approximately the same size as

those formed by buoyancy.

In order to show the close coupling of the buoyancy and surface tension forces in causing Bénard cells, Nield made a plot of the normalized Marangoni number, M/M_c, versus the normalized Rayleigh number, R/R_c, for parameters of $L = 0$ and $L = \infty$. L represents the free surface boundary conditions of the liquid film and is equal to zero for an insulating surface and infinity for a conducting surface. R/R_c and M/M_c represent the ratios of the energy available from buoyancy and the energy available from surface tension to the viscous dissipation energy required for the onset of turbulence, respectively. Nield points out that the small curvature in this plot, concave downward, shows that the coupling between the two agencies is tight but not perfect, since a small change in either M or R results in a change of the same order in the other. Nield indicated that the cells observed by Bénard were caused by surface tension since the critical Rayleigh number was not exceeded, but the critical Marangoni number was almost certainly exceeded.

Although the causes for movement at the interface of several different systems have been studied from different approaches and different mechanisms have been employed to explain the causes both qualitatively and quantitatively, there is good evidence from the above discussion that several of the mechanisms work in a combined effort to cause the motion. As has been pointed out by Nield (26) and Scriven and Sternling (34), there are mechanisms that dominate in causing interfacial motion for a given set of physical conditions; but the potential for either buoyancy driven or interfacial tension driven forces are present for all systems.

Although there have been several mathematical models presented from which the critical properties for causing interfacial turbulence in a given system can be determined, all contain assumptions that make it very difficult to devise experiments to directly check the results.

Two mechanisms, buoyancy and surface tension, have been employed both separately and together by several investigators in an attempt to explain quantitatively and qualitatively the interfacial motion observed in many liquid-vapor and liquid-liquid systems. Each mechanism has been concluded by different investigators to be the prime cause of interfacial movement observed in both liquid-vapor and liquid-liquid systems. Also, either temperature or concentration gradients in one or both phases of a system have been used to initiate the buoyancy or surface tension mechanism.

The author concluded that density variations as well as interfacial tension variations are the driving forces that produce interfacial turbulence. However, either density or interfacial tension may provide the dominant force for any given system. Also, it is concluded that the density variation or interfacial tension variations may be caused by a temperature or concentration gradient within the system.

Theory of Birefringent Interferometery

Olof Bryngdahl and Stig Ljunggren (4) have presented a paper describing a new, simple and versatile interferometer in which the interference fringes produce a direct plot of the refractive index gradient. They have presented the theory of the optical method in detail, together with an estimate of possible errors.

The arrangement of the optical system is presented in Figure 2. Bryngdahl and Ljunggren point out that the core of the method is formed by the two Savart birefringent plates, S_1 and S_2, together with the polarizers, P_1 and P_2.

The following is a very brief explanation of the function of the optical components of Figure 2. E represents an intense monochromatic light slit placed at the focal plane of the first lens L_1. Lens L_1 produces a collimated light beam which passes through the cell, then lens L_2 condenses the beam so that all rays may pass through the remaining optical components. Lens L_3 recollimates the light beam which passes through the first polarizer and Savart plate.

The Savart plate S_1 divides the rays of the plane polarized monochromatic collimated light beam into two components. The two components of each ray are separated in the vertical direction by a distance, b, which is a function of the Savart plate material and thickness. Therefore, for two rays separated vertically by a distance, b, in the condensed beam, a component from each ray will be recombined by the Savart plate S_1. When a concentration gradient exists within the cell, the recombined components can be out of phase by a given fraction of a wavelength. When the recombined rays are out of phase by n or $n \pm 1/2$ wavelengths, light and dark fringes are formed, respectively, for integral numbers of n. A more detailed explanation of the Savart plate is given by Strong (40).

Lens L_4 produces converging and diverging rays through the Savart plate S_2 and the polarizer P_2, respectively. The Savart plate S_2 divides the light rays horizontally into two components. The component from one light ray is then recombined with a component from a different

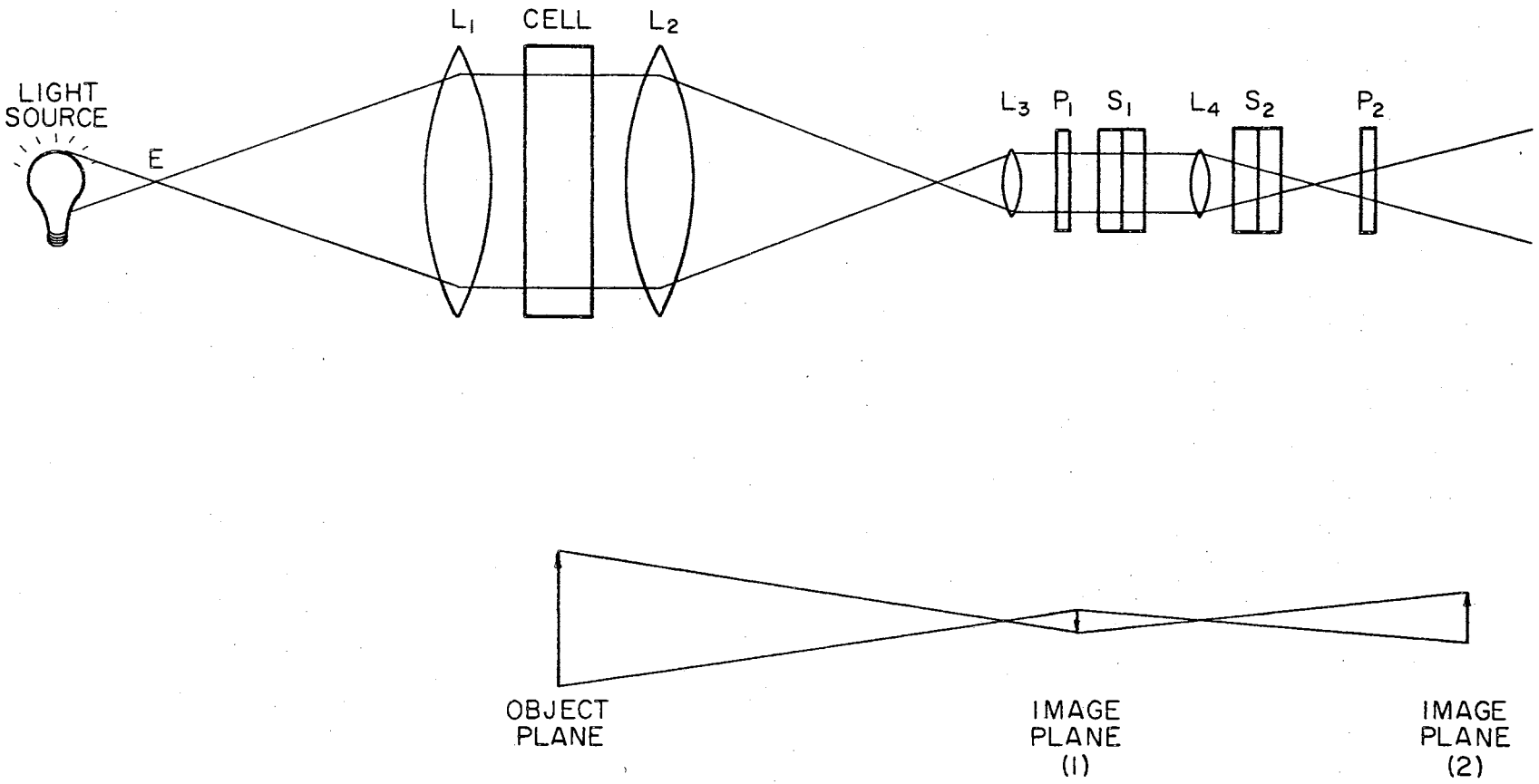

Figure 2. Birefringent Optical Arrangement

light ray. The Savart plate S_2 along with the polarizer P_2 form a series of vertical fringes visible in image plane 2. The fringes are caused by the constructive or destructive interference of the recombined ray components which are out of phase by an integral number of wavelengths or a half-integral number of wavelengths, respectively. The size and spacing of the fringes are a function of both the focal length of lens L_4 and of the Savart plate S_2 material and component thickness. If a refractive index gradient exists within the cell, each fringe pattern in image plane 2 will give directly the refractive index gradient as a function of position in the cell.

The converging rays on the Savart plate S_2 produce an angular displacement of the two wave fronts emerging from Savart plate S_1. This angular displacement causes a horizontal shift in the vertical fringes at the level where the refractive index in the cell is changing. The horizontal shift of the vertical fringes in the image plane 2 represents a plot of the refractive index gradient as a function of vertical position within the cell. Since the refractive index can be related to the concentration of the solution in the cell, the fringe pattern in the image plane 2 can be related to the concentration gradient as a function of vertical distance in the cell. A more detailed description with a mathematical representation of the interference of the light rays is presented by Bryngdahl and Ljunggren (4).

Bryngdahl (3) has presented the theories for two additional variations of the above optical system which employ the Savart plate in the Wavefront-Shearing Interferometer. These additional variations make use of modified Savart plates and of different rotations of the polarizers to the vertical and horizontal positions previously used.

The modification of the Savart plate allows the emerging rays to be plane polarized and to remain in the same plane as the original ray before division. This produces a greater separation of the split rays than is achieved by the conventional Savart plate of the same material and size.

CHAPTER III

EXPERIMENTAL APPARATUS

A birefringent interferometer, Figures 3 and 4, was used to measure a concentration gradient profile in the interfacial turbulence cell. This interferometer is a modification of the one constructed earlier (38) and is similar to the one used by Bryngdahl (4).

Interferometer Optical System

The optical system used for this study is described with aid of the schematic drawing, Figure 5.

The light source used was a Spectra-Physics helium-neon gas laser, Model 130, in place of the mercury vapor lamp used by Bryngdahl. The laser produces a monochromatic (6328Å), plane polarized with the electric vector in the vertical direction, and collimated light beam about 1.5 mm. in diameter with 0.005 watts power output. The light beam from the laser was expanded to about three inches in diameter and recollimated. The expanded light beam covered the interfacial turbulence cell so that the concentration gradient of the entire cell could be photographed.

The expansion and recollimation of the light beam was accomplished using two lenses: L_1, one-half inch in diameter with a 30 mm. focal length and L_2, three inches in diameter with a 1143 mm. focal length. L_1 was placed about two inches to the right of the laser

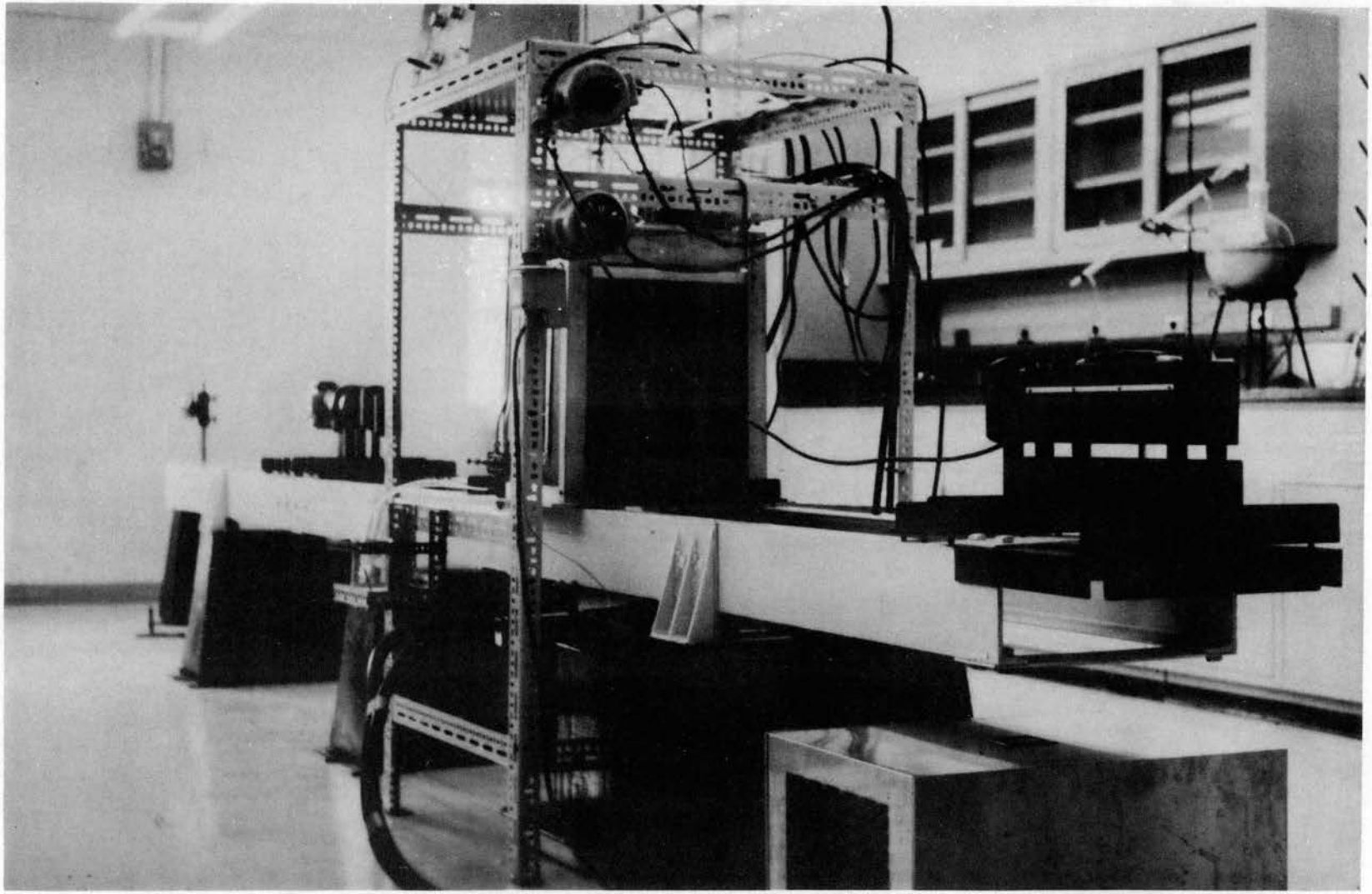

Figure 3. Light Source for Birefringent Interferometer

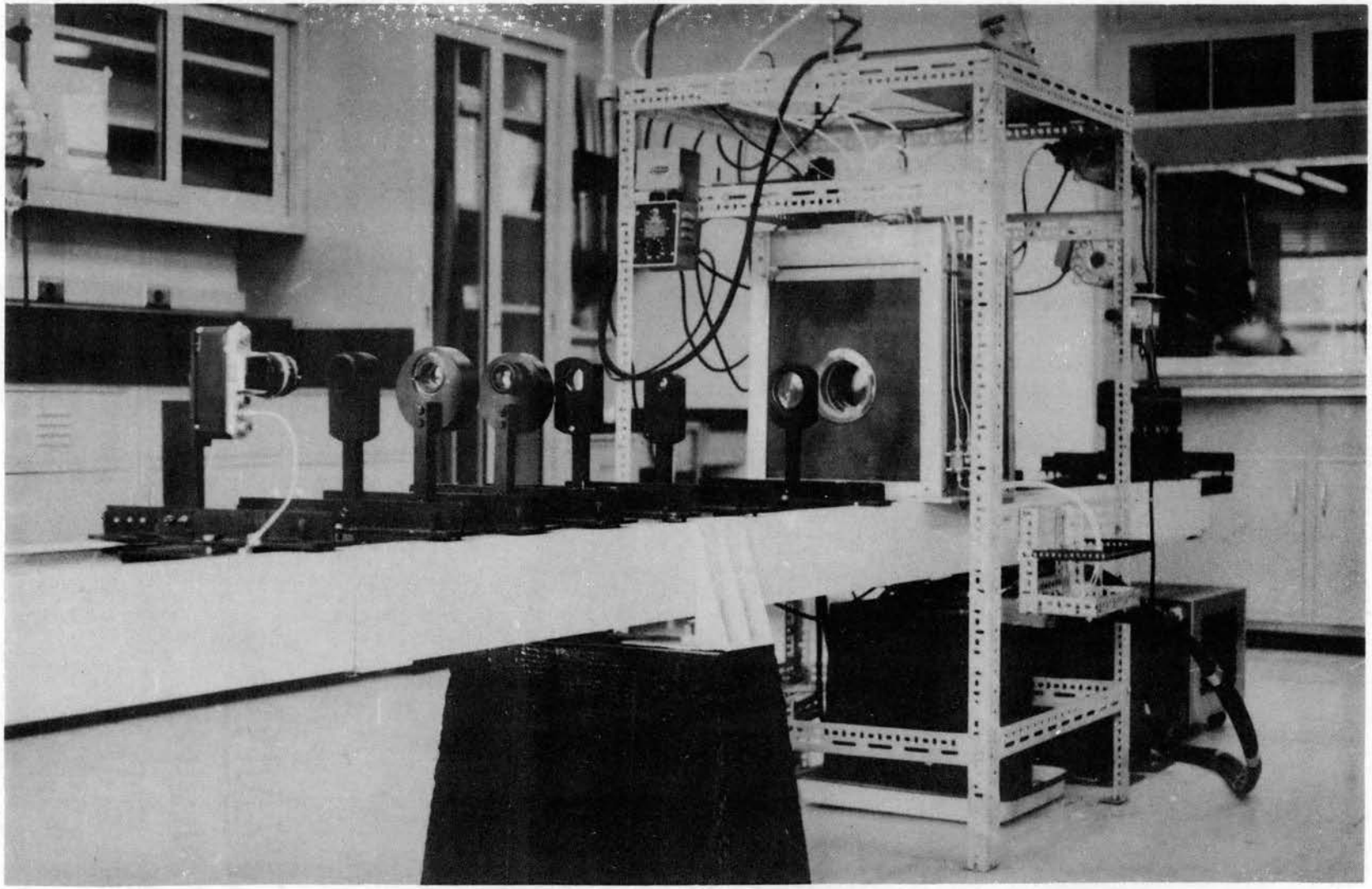

Figure 4. Optical Analyzer of Birefringent Interferometer

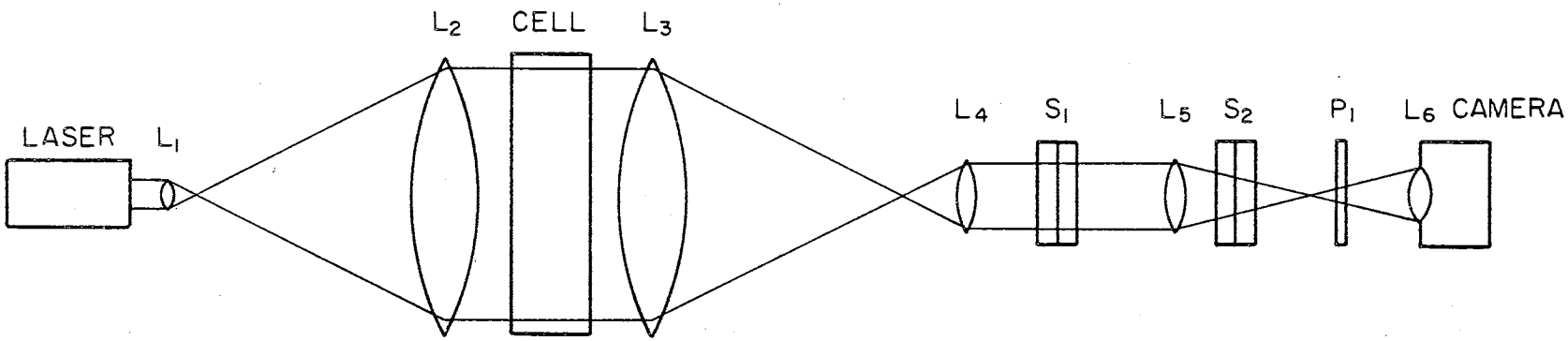

Figure 5. Optical Arrangement for This Study

output; and L_2 was placed 1,173 mm. to the right of L_1, which allowed the focal point of each to lie in the same plane.

The light beam was then contracted and recollimated in order that all rays of the light beam could be directed through a Savart plate. This was accomplished using two lenses: L_3, three inches in diameter with a 1143 mm. focal length and L_4, one-inch in diameter with a 140 mm. focal length. L_3 was placed two feet to the right of L_2 with L_4 placed 1283 mm. to the right of L_3 to produce collimated light.

The Savart plate, S_1, which was rotated to divide the ordinary and extraordinary rays of the light beam in the vertical direction was placed about three inches in front of L_4. The Savart plate S_1 was made up of two quartz crystal plates, each ten millimeters thick and one and one-half inches square, placed together with their optical axes at 90° to each other. The positioning of Savart plate S_1 between L_4 and L_5 is not critical.

Lens L_5 is one-half inch in diameter with a 50 mm. focal length. The positioning of L_5 along with the extension of the camera lens is used to achieve the desired magnification of the cell image. For this work, L_5 was placed about 245 mm. to the right of L_4. Also, the focal length of L_5 is critical in producing a given fringe size and spacing.

The Savart plate S_2, identical to Savart plate S_1, was placed about ten millimeters to the right of L_5 so that it would be traversed by converging light rays. Savart plate S_2 was rotated so it would produce vertical interference fringes. A plane polarizer with its electric vector in the horizontal plane was placed six inches in front of L_5. The positioning of the polarizer, P_1, between the Savart plate

S_2 and the camera lens is not critical.

A 35 mm. Nikon Model F camera, used to photograph the fringe pattern in the cell, was positioned to the right of the polarizer. The camera was equipped with a two-inch lens extension for magnification and was brought into focus on a plane one-third the cell thickness from the wall on the right side of the diffusion cell. This position of focusing was to produce sharper fringes according to Svensson (41). A motor drive attachment for the Nikon camera could be used for taking pictures up to a rate of four frames per second. The detailed optical alignment procedure used is presented in Appendix A.

Lenses L_2, L_3, and L_4 are compound lenses corrected for both chromatic and spherical aberrations and were purchased from Karl Lambrecht Crystal Optics. Lenses L_1 and L_5 are compound lenses corrected for chromatic aberrations and were purchased from Edmund Scientific Company. The polarizer, P_1, and two Savart plates, S_1 and S_2, were purchased from Karl Lambrecht Crystal Optics. The optical flats in the constant temperature water bath and the interfacial turbulence cell were cut from a piece of optical flat glass, cat. no. 2195, purchased from Edmund Scientific Company.

All the optical components were mounted on an optical bench with very rigid mounts built by the Research and Development Laboratory at Oklahoma State University. The mounts were designed so that the optical components could be adjusted in both the vertical and horizontal direction with rotational adjustment about the vertical and horizontal axes. The optical bench, 18 feet long by 16 inches wide, was constructed from six-inch by two-inch channel iron. Two pieces of the channel iron were bolted together in the shape of a ladder by seven,

four-inch by three-sixteenth inch iron strips equally spaced. The bench was cradled by three concrete pillars spaced six feet apart and three feet from each end of the bench. The concrete pillars were trapezoidal in shape, 24 inches by 12 inches at the base, 20 inches by eight inches at the top, 18 inches high, and weighed approximately 400 pounds each. The pillars were isolated from the high-frequency vibrations of the floor by two layers of one-quarter inch thick, two and one-fourth inch square Isomode vibration pads placed at each corner of the pillars.

Temperature Control System

A constant temperature water bath was mounted directly to the optical bench between lenses L_2 and L_3. The bath was constructed by the Research and Development Laboratory, Oklahoma State University. It consisted of a frame of one and one-fourth inch aluminum angle, an interliner of 22 gauge stainless steel, and an outside cover of three-sixteenths inch masonite. The bath was insulated with two inches of fiber glass. Two, six-inch by twelve-inch viewing windows on opposite sides of the bath were made from two layers of one-fourth inch Plexiglass separated by a three-fourths inch dead air space. The two sides of the bath in the optical path each had a four-inch diameter optically flat glass window. The optically flat windows were equipped with a three-point adjustment in order that they could be aligned.

The water in the bath was controlled by a Fisher Model 44 controller equipped with a thermistor probe sensing device. The deviations in temperature were observed on a Brooklyn Chemical thermometer, cat. no. 22214, calibrated at 20° and 30°C with 1/100° divisions from

18° to 30°C. The continuous heater, a 500-watt immersion type, W. H. Curtis Company No. 9668E, in conjunction with a Powerstat, Superior Electric type 116, and the control heater, a 200-watt immersion type, W. H. Curtain Company No. 9668C, were installed along one side of the bath with the thermistor probe placed about one inch in front of the heaters. A cooling coil, made from seven feet of one-fourth inch O.D. copper tubing with coils two inches in diameter, was installed along the same side of the bath. A three-gallon stone crock served as the cold sink from which water was circulated through the cooling coil by an Easy Industries, Easy Pump Model A-5. The temperature of the water in the cold sink was controlled by a Blue M Electric Company, Blue M cooler, Model PCC-1A. A Gerald K. Heller Company, electric controller 6T21 laboratory mixer with a variable shaft speed was installed between the heating and cooling coils of the constant temperature bath. All the auxiliary temperature control elements, except the cold sink and Blue M cooler, were mounted on a steel frame separated from the optical bench and the constant temperature bath. The cold sink and Blue M cooler were placed on the floor beneath the optical bench.

Interfacial Turbulence Cell

The interfacial turbulence cell, Figures 6 and 7, was of the flowing junction type and was constructed at the Research and Development Laboratory, Oklahoma State University. The cell was mounted inside the constant temperature water bath with a three-point adjustable mount to allow alignment of the cell. The cell was constructed of stainless steel with glass liners along two vertical walls and glass optical flats for the other two walls. The solution chamber was one

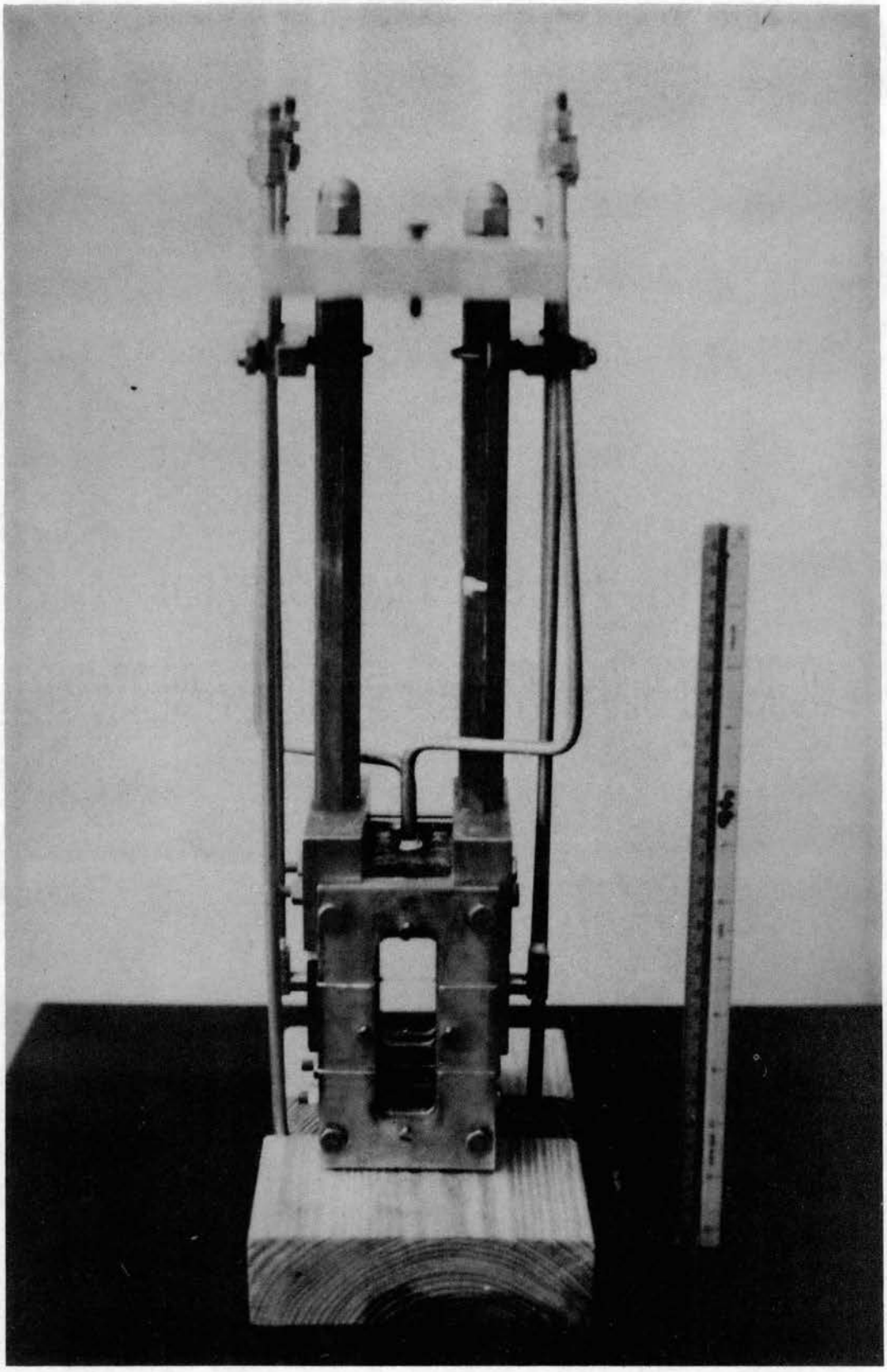

Figure 6. Interfacial Turbulence Cell

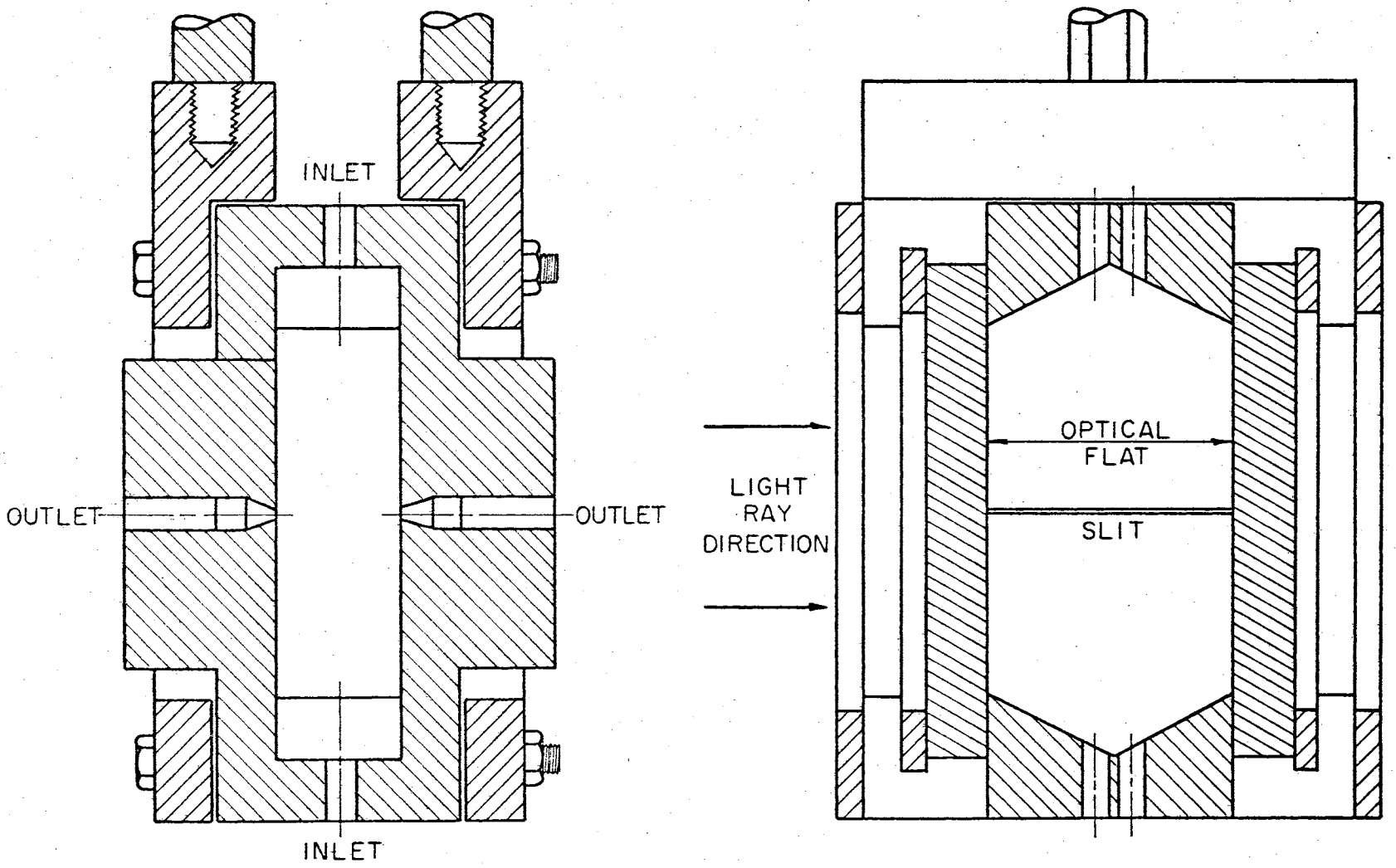

Figure 7. Cross-Section of Interfacial Turbulence Cell

inch wide, two inches deep (along the optical path), and four inches high with a funnel-shaped top and bottom to prevent the trapping of air. The solution tanks were 125 milliliter glass separatory funnels; and the feed and discharge lines, equipped with one-fourth inch stainless steel needle valves, were of one-fourth inch teflon tubing. The cell had two openings in the top and in the bottom; each opening was one-eighth inch in diameter. It also had an opening, at the center, in the two stainless steel sides. Each opening was a 0.006-inch slot, two inches long. All the openings were fitted with stainless steel Swagelok fittings and arranged so that any opening could be used for discharge or feed.

Auxiliary Equipment

The optical system of the interferometer was aligned with an alignment telescope, Figure 8. The telescope, from Gaertner Scientific Corporation, was 17 power and was equipped with a cross-hair, a sensitive leveling bulb, and a Gauss eye-piece. The telescope was mounted on a stand made from a stainless steel bar one inch in diameter with a 150-pound concrete base. The stand could be leveled by three adjusting screws at its base; and the telescope could be raised, leveled, and rotated about the stainless steel bar.

Concentrations for aqueous uranyl nitrate solutions were analyzed with a Bausch and Lomb precision refractometer, from Bausch and Lomb, Inc., which is a modification of the Abbe type. With the precision refractometer, the concentrations of the solutions were determined to within ± 1 percent. The solution concentration was determined from a plot of refractive index versus solution concentration. The plot was

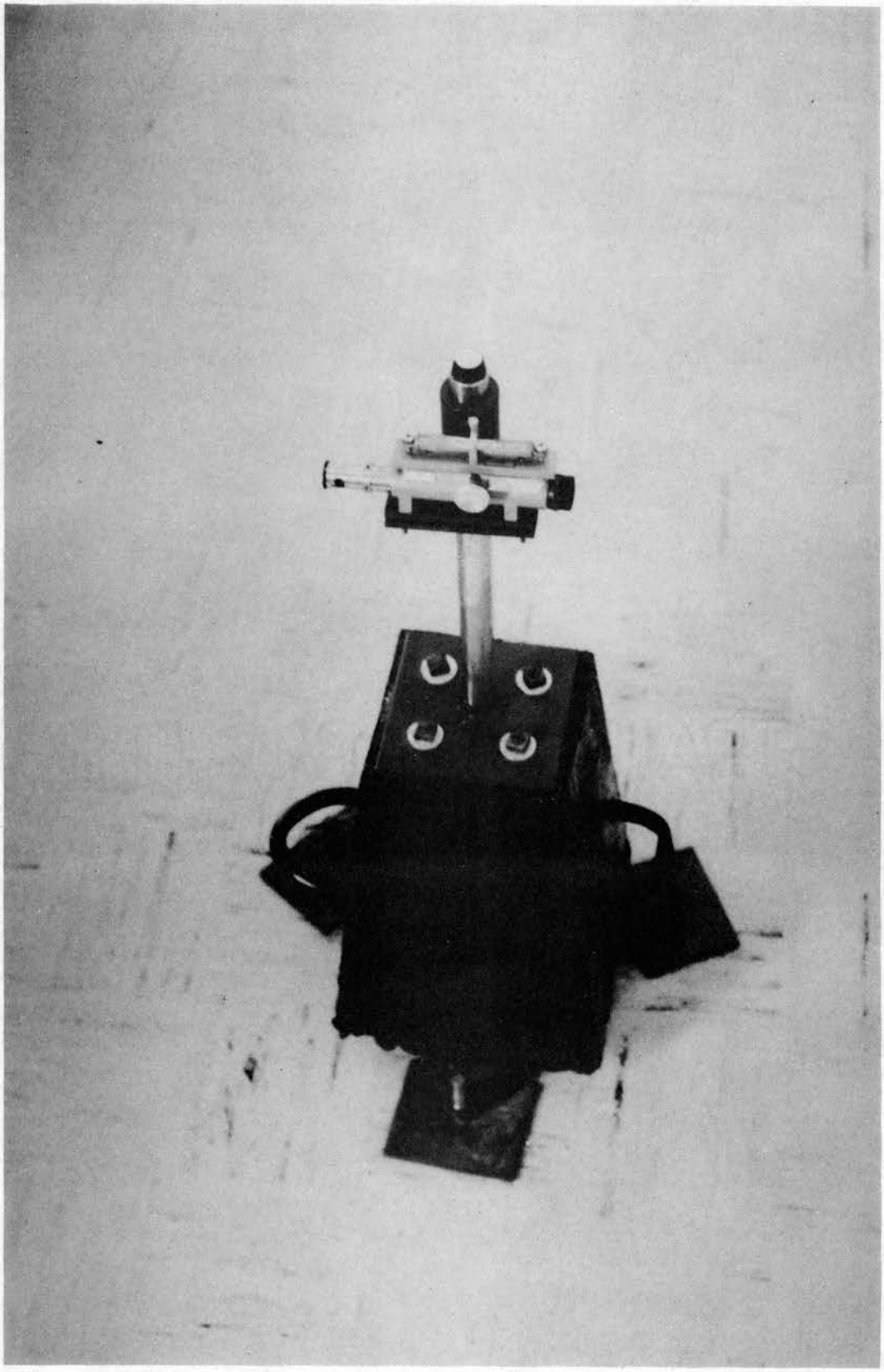

Figure 8. Alignment Telescope

made using standard solutions prepared by measuring the water in volumetric flasks and weighing the uranyl nitrate hexahydrate crystals on a Mettler Gram-atic Semi-Micro Balance, Type B6, with an accuracy of ±0.00002 grams. The refractive index measurements were made at 25 ± 0.1°C.

CHAPTER IV

EXPERIMENTAL PROCEDURE

The steps followed in obtaining data for the study of interfacial turbulence between two immiscible liquids using the birefringent interferometer are (1) the solutions are prepared and analyzed, (2) the interfacial turbulence cell is prepared for the run, (3) the chamber of the interfacial turbulence cell is filled and adjusted, (4) the solutions are brought to constant temperature, (5) photographs of the fringe pattern are taken, and (6) data are collected from the photographs. A detailed explanation of each step is presented in the following paragraphs:

Preparation and Analysis of Solutions

The water used in each of the systems was triple-distilled to remove surfactants. Triple-distilled water was made by starting with four liters of distilled water obtained from a Barnstead Water Still, cat. no. EMQ-5, Barnstead Still and Sterilizer Company (laboratory supply). The four liters of distilled water were made slightly acidic by adding four or five drops of concentrated sulfuric acid and about one gram of potassium permanganate crystals or enough to form a dark purple color. This solution was distilled with the first 400 milliliters and the last 1,000 milliliters being discarded. The center cut was then made slightly basic with about one-fourth gram of barium

hydroxide and redistilled. The first 400 milliliters and the last 600 milliliters of water were discarded, and the center cut of this distilling was taken as triple-distilled water. The still consisted of a five-liter round bottom flask, an electrical heating mantle with a Powerstat control, and a double-tube glass condenser affixed to the round bottom flask with polyethylene stoppers. The triple-distilled water was then stored in glass bottles that had been rinsed with triple-distilled water. This procedure is similar to that given by Shoemaker and Garland (37).

The tributyl phosphate (TBP) used in this work was purified by the following procedure to remove degenerated complexes of the tributyl phosphate: One-thousand milliliters of commercial grade TBP, purchased from Commercial Solvents Corporation, were boiled in 500 ml. of sodium hydroxide (0.5 molar) for ten hours with total reflux and then for one hour with no reflux. The TBP was then washed five times, with triple-distilled water, until the wash water remained neutral. About 500 ml. of hot water were used for each washing. This procedure is outlined by Lewis (20).

The acetone and toluene used in this work were technical grade and were not further purified.

Three separate solutions were required in order to make an interfacial turbulence run for one system. Two of the solutions are miscible with one at a higher solute concentration than the other, while the third is immiscible with the first two but in equilibrium with the one of lower solute concentration.

For the water-acetone-toluene systems, acetone is the solute transferred from the organic phase (acetone-toluene) to the aqueous

phase (acetone-water). In preparing the immiscible solutions, volumetric measurements of each component were mixed in a four-liter separatory funnel. After phase equilibrium was obtained, the aqueous and organic phases were separated; and the acetone concentration in each phase was estimated with the aid of an equilibrium diagram for water-toluene-acetone (41). The third solution was then prepared by adding to a volumetric portion of the organic phase an additional volumetric amount of acetone.

For the water-uranyl nitrate-TBP-n-heptane system, uranyl nitrate is the solute transferred from the aqueous phase (uranyl nitrate-water) to the organic phase (uranyl nitrate-TBP-n-heptane). In preparing the immiscible solutions, volumetric amounts of water, TBP, and n-heptane were mixed in a four-liter separatory funnel with a weighed amount of uranyl nitrate hexahydrate crystals. After equilibrium was reached, the organic and aqueous phases were separated; and the uranyl nitrate concentration of the aqueous phase was determined from a measure of the solution refractive index with the Bausch and Lomb precision refractometer. The uranyl nitrate concentration of the organic phase was then determined from a material balance calculation, taking into account the six moles of water present for every mole of uranyl nitrate in the crystalline form. The third solution was then prepared by adding to a volumetric portion of the aqueous phase an additional amount of uranyl nitrate hexahydrate crystals.

The volumetric measurements were made using volumetric flasks and pipettes, and the weight of the uranyl nitrate hexahydrate crystals was determined using a Mettler balance.

Preparation and Mounting of Cell

In preparing the interfacial turbulence cell for a given run, it was carefully cleaned according to the procedure detailed in Appendix B. When the cell had been properly cleaned, it was lined with the particular lining determined by the type of system being used. There were two types of glass liners used in the cell: one type was preferentially wet by the organic solution, and the other type was preferentially wet by the aqueous solution. The lining selected was the one preferentially wet by the solution from which the solute was transferred. This allows the parabolic-shaped interface between the two phases to convex into the solution from which the solute was transferred. Once the cell was lined with the proper lining and the optical flats had been affixed leak tight to the cell chamber, the cell was placed into the constant temperature bath and aligned according to the procedure in Appendix A.

Filling of Cell

When filling the cell with the liquids to be tested, the more dense solution was always fed into the bottom of the cell. For interfacial turbulence studies, there are, in most cases, three sections of liquids in the cell chamber, similar to that shown in Figure 9.

Liquid phase O is miscible with liquid phase P but of higher solute concentration, while liquid phases P and Q are immiscible but in phase equilibrium. The higher density phase was added first when possible. For this example, phase O was added first through feed line 5. The phase was added slowly, in order to remove all air from feed line 5, while venting feed line 1 or 2. Phase O was added until it

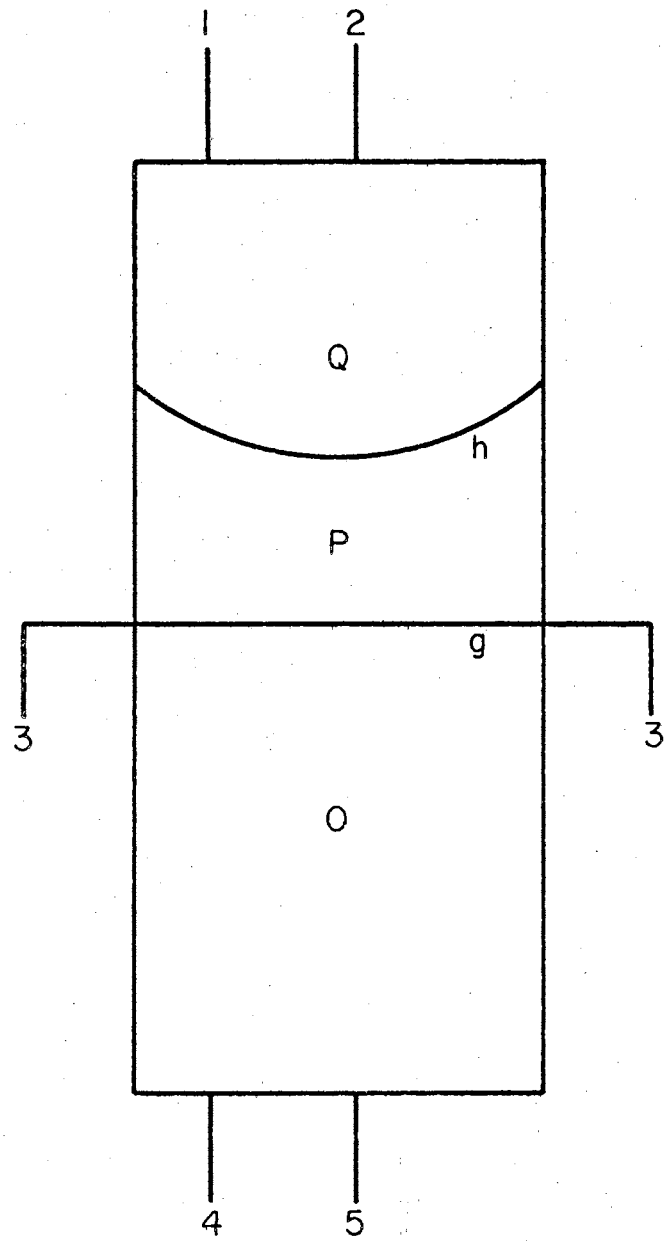

Figure 9. Interfacial Turbulence Cell Chamber

filled the lower half of the cell chamber. Then phase P was added very slowly through feed line 1 by venting feed line 2. Solution was then drawn off through lines 3, in order to drive the air from these lines. It was important that the air be removed from lines 3 before the chamber had been completely filled so that no air would be forced back into the cell chamber after it had been filled. Phase P was allowed to completely fill the cell chamber, driving all air from lines 1 and 2. It was important that all the air be removed from the cell chamber and lines so that a smooth, steady flow could be obtained.

In filling the cell, a mixture of phase P and O would result in the cell chamber and feed line 2. This mixture was removed from feed line 2 and the upper half of the cell chamber by adding about 100 $cm.^3$ of phase P through feed line 2. Phase P was added slowly by drawing off solution through lines 3 at a rate of one drop per second from each line. The mixture of phase P and O was removed by adding about 50 $cm.^3$ of phase O through feed line 5 in the above manner. Note that only one phase was added at a time while filling the cell and that the discharge line was closed when changing feeds from one feed line to another.

Phase Q was added to the cell chamber through feed line 2 by drawing off solution through the discharge lines at a rate of one drop per second from each line. Phase Q is immiscible and in equilibrium with phase P. Therefore, there was no net diffusion between these phases as phase Q was added. When phase Q first entered the cell chamber, the flow from the discharge lines was stopped. The solution tanks 2 and 5 were then adjusted to predetermined levels in order to obtain an equal liquid head for the two tanks. The levels of the

solution tanks were estimated from the density of phases O and Q before attempting the adjustment. It was important that the level of the liquid in each tank be at the same height within the tanks so that the same flow rate for each phase could be achieved.

With the solution tanks adjusted for equal liquid head, the flow was resumed from feed lines 2 and 5 simultaneously. The flow rate was set by adjusting the discharge rate through lines 3 at one drop every two seconds. This flow rate will allow a sharp interface, g, between phases O and P to be obtained and allow the interface, h, between P and Q to approach interface g very slowly.

There were two separate procedures followed from this point. First, the flow was continued until phase Q was being drawn through each discharge line or until interfacial turbulence was observed, whichever came first. Second, the flow was continued only until interface h approached interface g within about one-eighth of an inch. The solute was then diffused across phase P to interface h causing a solute concentration gradient along interface h. This latter procedure was conducted only for observation purposes since the concentration gradient could not be calculated using the existing optical system. The concentration gradient required to cause interfacial turbulence was so large that the fringes produced by the existing optical system were blurred together and thus could not be measured.

Control of Temperature

The constant temperature water bath was controlled at 25°C ± 0.005°C. This was accomplished with the equipment housed in a temperature-regulated room at 24°C ± 1°C. The water in the bath was

heated by a 500-watt immersion heater which was on continuously and by a 200-watt immersion heater on control. The water in the bath was cooled by circulating cooling water through a copper coil immersed in the bath. The cooling water was controlled at 10°C ± 1°C in the cold sink by a Blue M refrigeration unit. In order to obtain a uniform on-off time for the control heater, both the cooling water flow rate and the voltage to the continuous heater were adjusted. The solutions in the interfacial turbulence cell were assumed to be in thermodynamic equilibrium at 25°C, since the time required to sharpen the interface was about two hours and very little solution replacement was required for this process.

Photographing of Fringe Pattern

For the first procedure followed, three photographs were taken for each run. The first photograph was taken when the interface h was about half-way between the top and center of the cell chamber. The second photograph was taken shortly before interface h came into contact with interface g, and the third photograph was taken at the termination of the run. The time was recorded when each photograph was taken.

For the second procedure followed, photographs were taken at evenly spaced intervals (10, 20, or 30 seconds) until interfacial turbulence was observed. The first photograph was taken as soon as the discharge lines were closed and recorded as time zero.

Collection of Data From Photographs

The photographs taken during the experimental run for the major

part of this study were to verify both the solution flow rate from the cell and the contact of interface h with interface g, Figure 9. Three photographs were generally taken during a run.

The distance between interface h and interface g was measured from each of the first two photographs using the toolmaker's microscope. (The toolmaker's microscope is described in Appendix D.) These distances were corrected for magnification in order to determine the separation of the two interfaces within the cell chamber. (The procedure for obtaining magnification is outlined in Appendix D.) The velocity at which the interface h approached the center of the cell was calculated from these two measurements and using the time recorded when the photographs were taken. The third photograph was taken to verify that contact had been made between interface h and g.

A series of photographs taken during one of the runs for a TBP-n-heptane-uranyl nitrate-water system is presented in Figure 10. Photographs 1 and 2 were taken during the time that a steep concentration gradient was being produced at the aqueous-aqueous interface. The horizontal fringe at the center of each photograph represents the aqueous-aqueous interface. Photograph 3 was taken after contact had been made between the aqueous-organic interface and the aqueous-aqueous interface. The concave fringe in the top half of each photograph represents the aqueous-organic interface. This series of photographs was taken for a system with an organic phase uranyl nitrate concentration of 0.066 molar in equilibrium with an aqueous uranyl nitrate concentration of 0.0997 molar. The step uranyl nitrate concentration difference was 0.0727 molar. Interfacial turbulence was observed during this run; however, the turbulence did not show up in

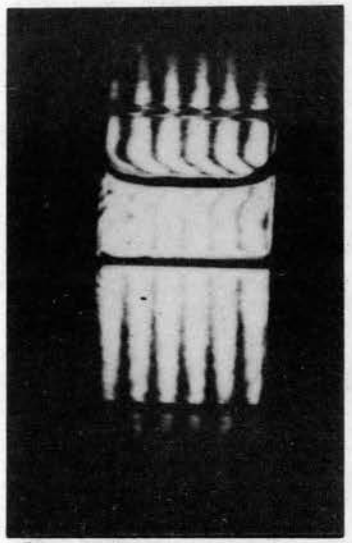

1. Time = 0 sec.

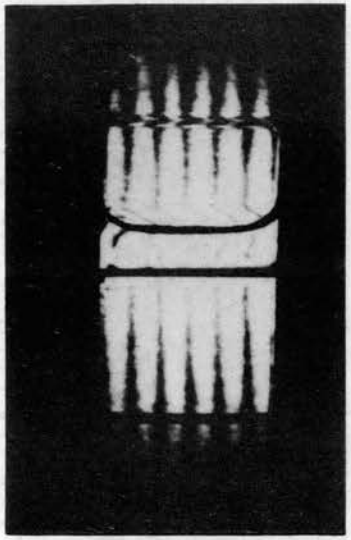

2. Time = 600 sec.

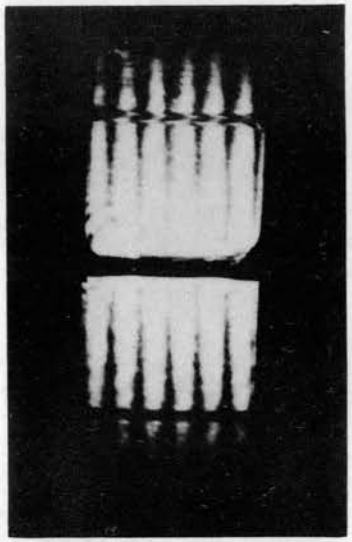

3. Time = 1,235 sec.

Figure 10. Photographs of Interfacial Turbulence in a TBP-n-Heptane-Uranyl Nitrate-Water System

photograph 3.

CHAPTER V

RESULTS AND DISCUSSION

This work was conducted in order to develop experimental techniques for studying interfacial turbulence and to learn something of the physical phenomena which initiate interfacial turbulence along a liquid-liquid interface between two immiscible liquids. The birefringent interferometer was selected to measure the concentration gradient as a function of position within the cell chamber at the onset of interfacial turbulence. In order to work out an experimental procedure for this study, a system of toluene-acetone-water was used. The system toluene-acetone-water was chosen for a preliminary study, since it has been reported by several investigators to produce interfacial turbulence (15, 16, 21). A tributyl phosphate-n-heptane-uranyl nitrate-water system was used to study the physical phenomena which initiate interfacial turbulence.

Toluene-Acetone-Water System

One phase of this study was to determine what effect a solute concentration gradient along the liquid-liquid interface would have on the initiation of turbulence. Therefore, the experiments were conducted so that a solute concentration gradient along the liquid-liquid interface between the two immiscible phases could be produced. This was accomplished by forming a convex interface between the two

immiscible phases and allowing a plane solute gradient to diffuse into the convex interface. The method was tested using the toluene-acetone-water system and found to produce turbulence only when a very steep acetone gradient was allowed to diffuse into the interface between toluene and water. The gradient required to produce interfacial turbulence for this system, as well as for the tributyl phosphate-n-heptane-uranyl nitrate-water system, was so great that the concentration of solute as a function of cell chamber position and thus the concentration gradient along the toluene-water interface could not be measured with the existing optical system. For the steep concentration gradients required to produce turbulence, the fringe spacing was so close at the interface that individual fringes could not be distinguished and measured.

Figures 11A, 11B, 11C, and 11D present a series of photographs of the cell chamber during an interfacial turbulence study of the toluene-acetone-water system. These photographs were taken of the center section of the cell chamber and show the flat interface between the toluene and toluene-acetone mixture and the convex interface between the water and toluene. Only a circular portion of the cell is shown due to the use of a circular camera lens with very large magnification. The light area in the photographs below the dark wide curved line in the horizontal direction (organic-aqueous interface) represents the aqueous phase. This phase corresponds to the phase Q in Figure 9 which is the phase into which the solute (in this case acetone) is transferred. The dark wide horizontal line, which is located above the curved line, represents the interface between the two miscible organic phases. The portion above the horizontal line represents the

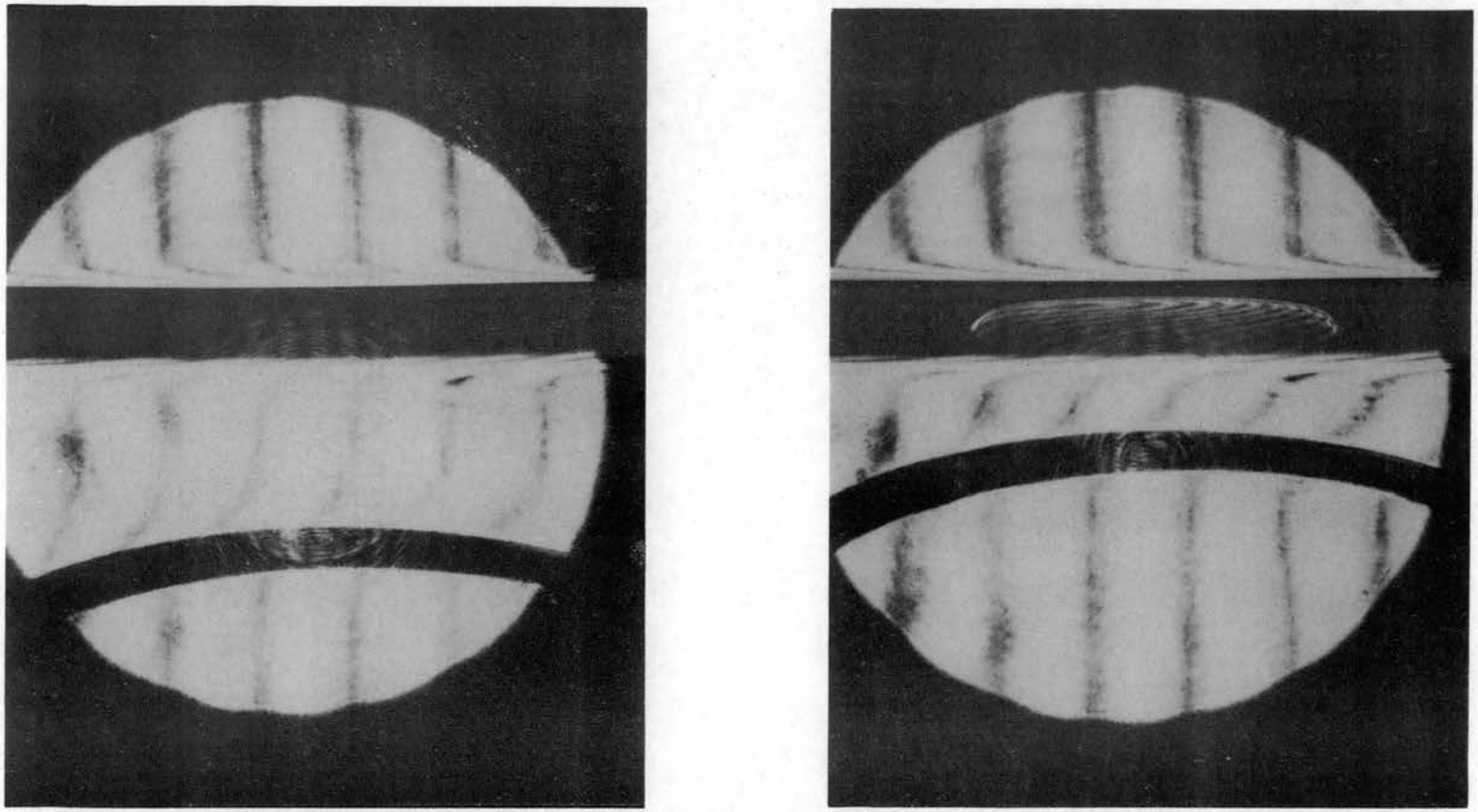

1. Time = 0 sec.

2. Time = 90 sec.

Figure 11A. Photographs of Interfacial Turbulence in a Toluene-Acetone-Water System at 0 and 90 Seconds

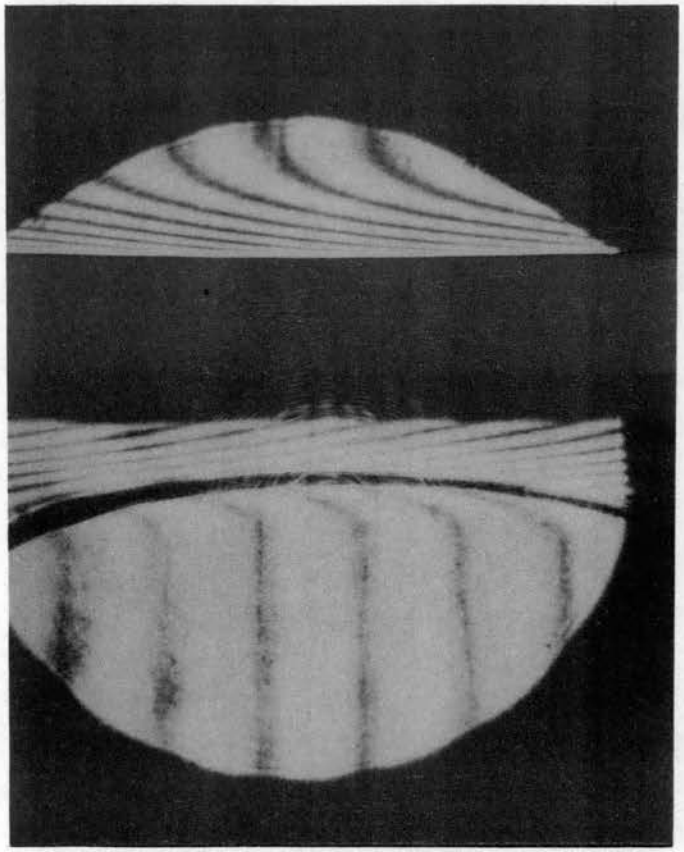

3. Time = 180 sec.

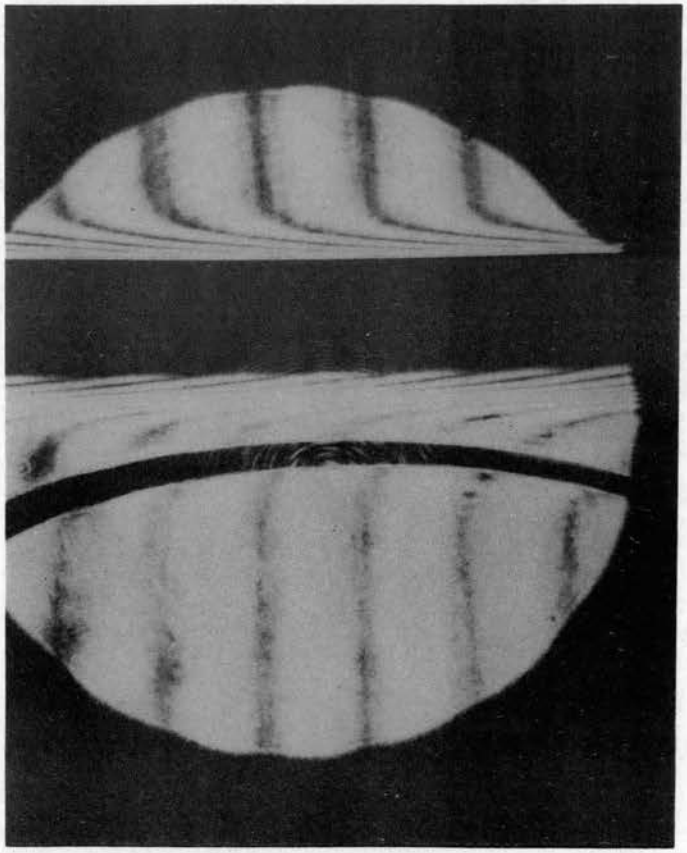

4. Time = 540 sec.

Figure 11B. Photographs of Interfacial Turbulence in a Toluene-Acetone-Water System at 180 and 540 Seconds

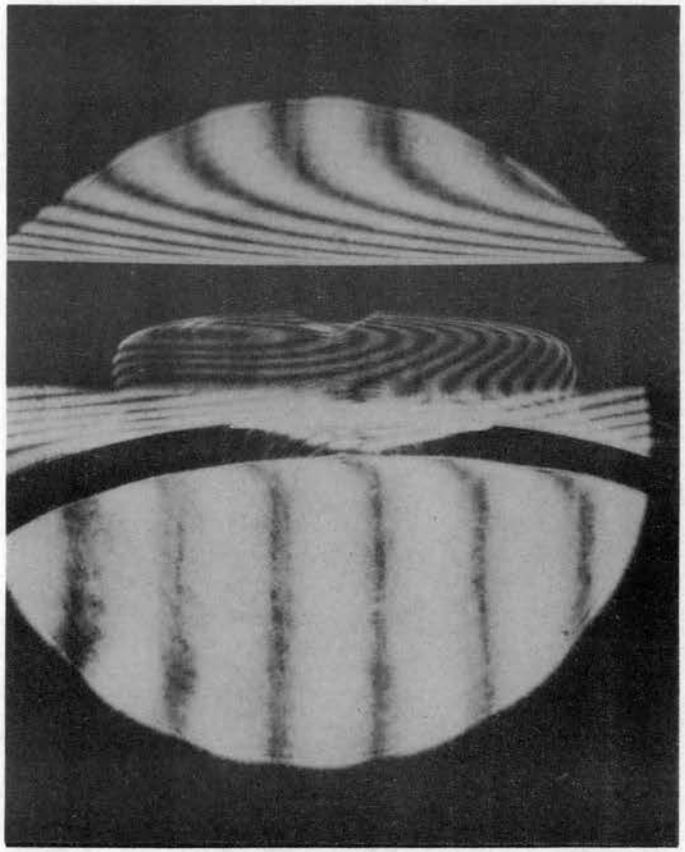

5. Time = 570 sec.

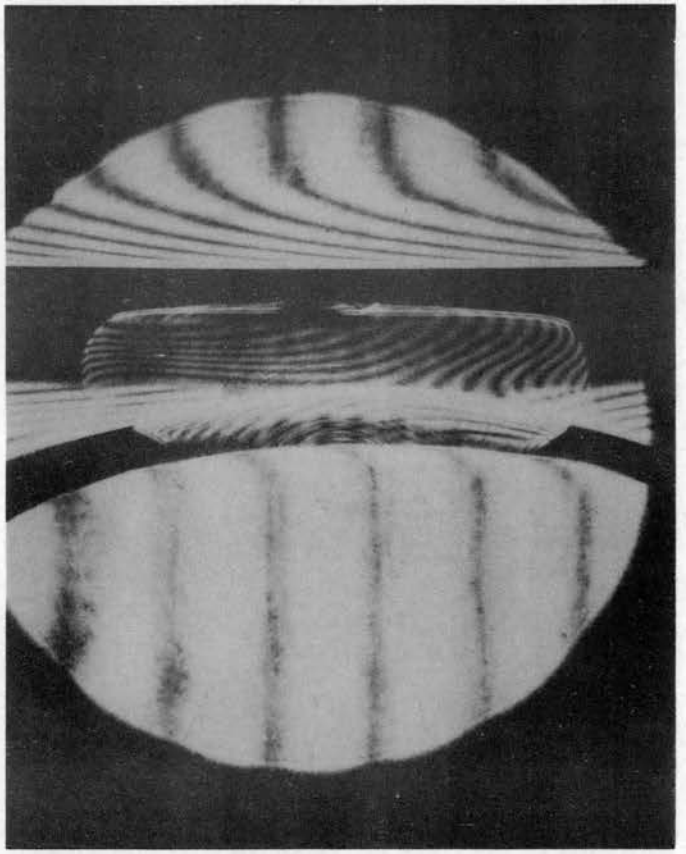

6. Time = 600 sec.

Figure 11C. Photographs of Interfacial Turbulence in a Toluene-Acetone-Water System at 570 and 600 Seconds

7. Time = 630 sec.

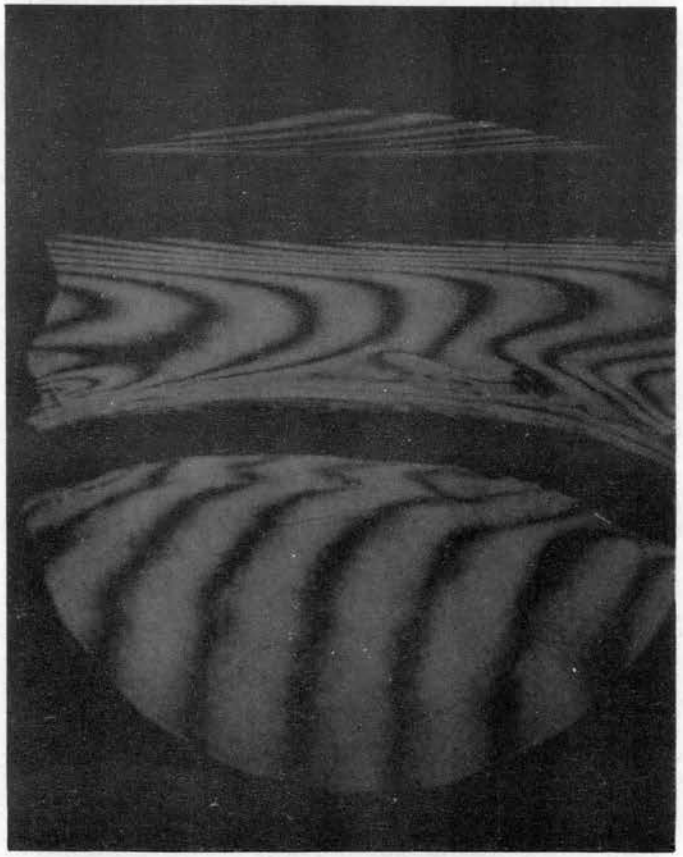

8. Time = 780 sec.

Figure 11D. Photographs of Interfacial Turbulence in a Toluene-Acetone-Water System at 630 and 780 Seconds

toluene with a low acetone concentration and corresponds to phase P in Figure 9. The vertical black lines in the photographs are the fringes produced by the interferometer and represent the refractive index gradient as a function of position in the cell chamber. These fringes are related to the concentration gradient in the cell chamber by a straight line relation between the concentration and refractive index. The fringes curve at the aqueous-organic interface and at the organic-organic interface. The straight portion of the fringes represents the region in both solutions for which the rate of change in acetone concentration is zero. The horizontal displacement of the vertical fringes near the interface is proportional to the rate of change of acetone concentration in this region.

Photograph 1, labeled time = 0 seconds, was taken while the organic-organic interface was being sharpened. The fringe pattern shows that the concentration gradient changes at only a very short distance either side of the two interfaces. Photograph 2, labeled 90 seconds, was taken 90 seconds after flow to and from the cell had been stopped. The oval-shaped fringe pattern near the center of the organic-organic interface indicates a slight distortion of the interface between the solutions in that region. This phenomenon could not be observed by looking directly into the cell chamber.

From photographs 2, 3, and 4, it is seen that the organic-organic interface becomes wider and that the vertical fringes become curved at a greater distance from the organic-organic interface. This is caused by the diffusion of the acetone across the organic-organic interface. In photograph 4 the curvature of the fringes below the aqueous-organic interface indicates that the acetone is beginning to be transferred

into the aqueous phase.

In photographs 5 and 6, the oval-shaped fringe patterns reappear at the center of the organic-organic interface. This represents the onset of turbulence which is shown fully developed in photograph 7. The turbulence shown in photograph 7 can readily be observed by looking directly into the cell chamber at this time. Photograph 8 shows the system as turbulence subsides. It is noted that the distance between the aqueous-organic interface and the organic-organic interface is greater than before turbulence was initiated. This is caused partly by the depletion of acetone and partly by the mixing of the upper organic phase during turbulence.

Since the concentration gradient along the toluene-water interface could not be determined for those systems producing turbulence, an alternate method was used to measure the minimum gradient required to produce turbulence. This was accomplished by bringing the convex toluene-water interface into contact with the sharp flat interface between the toluene and toluene-acetone mixture. A step concentration difference along the toluene-water interface was thus produced and the minimum step concentration difference required to produce interfacial turbulence obtained by successive experiments until a step difference was found for which no turbulence was observed. This method would not provide the actual minimum gradient required to produce interfacial turbulence for a given system, but it would provide a relative gradient from which different systems could be compared.

It was hoped that this apparatus could be used to determine the effect that the direction of solute transfer had on the initiation of interfacial turbulence, since Lewis (21) stated in his work that some

systems produced turbulence for transfer of solute in one direction but did not produce turbulence for transfer of the solute in the reverse direction. However, this was impossible for the systems used in this investigation, since the systems were density stable for solute transfer in only one direction. For the toluene-acetone-water system, only for acetone transfer from toluene to water was the system density stable. When an attempt was made to transfer acetone from water to toluene, a sharp interface could not be obtained between the water-acetone mixture and the water because of mixing due to density differences. The water-acetone mixture had to occupy the lower chamber of the cell and it was less dense than the pure water above it. Therefore for this work, only density stable systems were studied.

Tributyl Phosphate-n-Heptane-Uranyl Nitrate-Water

The causes of interfacial turbulence when uranyl nitrate is transferred from the aqueous phase into the organic phase were investigated by determining the minimum uranyl nitrate concentration differences across the interface required to produce turbulence. The minimum concentration difference or range of differences required to produce turbulence was determined for several aqueous phase concentrations of uranyl nitrate in equilibrium with the organic phase. A tabulation of the range of differences and of the concentrations is given in Table VI of Appendix F. The range of differences gives the step concentration difference for which interfacial turbulence was not observed and a higher step concentration difference for which interfacial turbulence was observed. Therefore, the minimum step concentration difference required to cause interfacial turbulence in a

system is located within the range of differences.

The equilibrium concentration of uranyl nitrate in the organic phase was determined from an equilibrium plot, Figure 20 given in Appendix E. The equilibrium concentration of uranyl nitrate in the organic phase, obtained from Figure 20, is presented in Table I for each concentration and range of step concentration differences used in this study. The organic phase concentrations used to construct Figure 20 were obtained from material balance calculations for which volume changes in the aqueous and organic phases were not considered (8).

From a plot of the range in aqueous phase step concentration differences required to produce turbulence versus aqueous phase concentration of uranyl nitrate, Figure 12, it can be seen that the minimum aqueous phase step concentration difference required to cause turbulence is nearly constant for all systems except at the 0.77 molar uranyl nitrate aqueous phase concentration. However, the high step concentration difference required to produce turbulence at the 0.77 molar aqueous phase concentration would indicate that the rate of solute transfer was not the major cause of turbulence, since the rate of transfer should be more for a larger concentration difference. This would agree with Haydon's (16) statement that heat effects are at most second order, since for a smaller rate of transfer there would be a smaller rate of heat generated due to reaction. However, since the rate of transfer is a function of the step concentration differences and the diffusion coefficient in each phase, Figure 12 does not give a quantitative comparison of the rate of solute transfer for each system.

The interfacial tension and the range of step interfacial tension differences required to produce turbulence for the TBP-n-heptane-

TABLE I

AQUEOUS AND ORGANIC PHASE URANYL NITRATE CONCENTRATION DIFFERENCE REQUIRED FOR TURBULENCE

System No.	Equilibrium $UO_2(NO_3)_2$ Conc.		$UO_2(NO_3)_2$ Conc. Difference for Which Interfacial Turbulence Was Not Observed		$UO_2(NO_3)_2$ Conc. Difference for Which Interfacial Turbulence Was Observed	
	Aqueous Molar	Organic Molar	Aqueous Molar	Organic Molar	Aqueous Molar	Organic Molar
1	0.0000	0.0000	0.07008	0.022	0.08971	0.052
2	0.0997	0.066	0.0209	0.037	0.0314	0.050
3	0.2037	0.196	0.0385	0.032	0.0578	0.048
4	0.3754	0.308	0.0387	0.017	0.0489	0.021
5	0.5472	0.367	0.0545	0.013	0.0725	0.018
6	0.7700	0.415	0.1766	0.026	0.2570	0.035

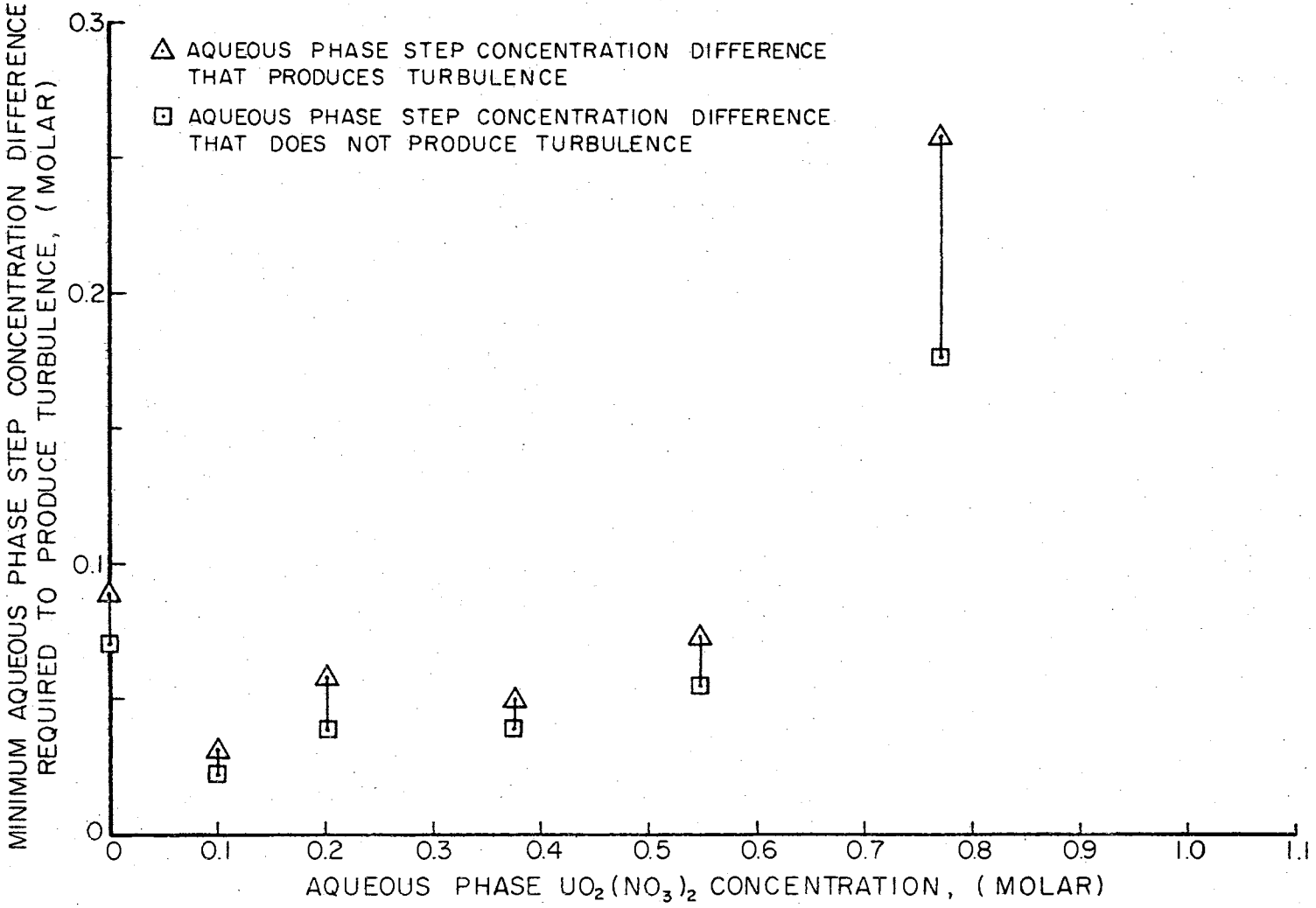

Figure 12. Step Concentration Differences Required for Turbulence

uranyl nitrate-water systems are presented in Table II. The interfacial tension values were obtained from a plot of interfacial tension versus aqueous phase concentration of uranyl nitrate, Figure 21 in Appendix E.

From a plot of the range of step interfacial tension differences required to produce turbulence versus aqueous phase concentration of uranyl nitrate, Figure 13, it is seen that a nearly constant minimum step interfacial tension difference is required for each concentration. Some of the variations in the step interfacial tension difference required to produce turbulence might be explained by experimental error as well as by error in the interfacial tension data. However, this variation in the minimum step interfacial tension difference required to produce turbulence indicates that interfacial turbulence is a function of the step interfacial tension difference as well as other parameters.

In order to study the causes of interfacial turbulence as a function of the interfacial tension gradient as well as other parameters, the experimental data obtained in this work have been evaluated from equations derived by Marsh, Sleicher, and Heideger (23). Values of the disturbance factor as a function of the system's physical properties were computed from Equation 1 of Chapter II. Equation 1, neglecting the surface viscosity term, was solved on the 7040 IBM computer using a program obtained from Marsh (23). Since Marsh had programmed the equation for a hypothetical case, slight modifications were required in order to apply the experimental data, Table III, to the program in Appendix G. This included reading into the program experimental values for the concentration and the coefficient of

TABLE II

INTERFACIAL TENSION DIFFERENCE REQUIRED

FOR TURBULENCE

System No.	Aqueous Phase Conc. $UO_2(NO_3)_2$ Molar	Interfacial Tension dyne/cm.	Interfacial Tension Difference for Which Turbulence Was Not Observed dyne/cm.	Interfacial Tension Difference for Which Turbulence Was Observed dyne/cm.
1	0.00000	11.90		
	0.07008		0.50	
	0.08971			0.64
2	0.0997	12.61		
	0.1206		0.20	
	0.1311			0.29
3	0.2037	13.71		
	0.2422		0.49	
	0.2615			0.78
4	0.3754	16.50		
	0.4141		0.74	
	0.4243			0.90
5	0.5472	19.01		
	0.6017		0.55	
	0.6197			0.71
6	0.7700	20.85		
	0.9466		0.95	
	1.0270			1.27

Note: Interfacial tension values are obtained from Figure 21.

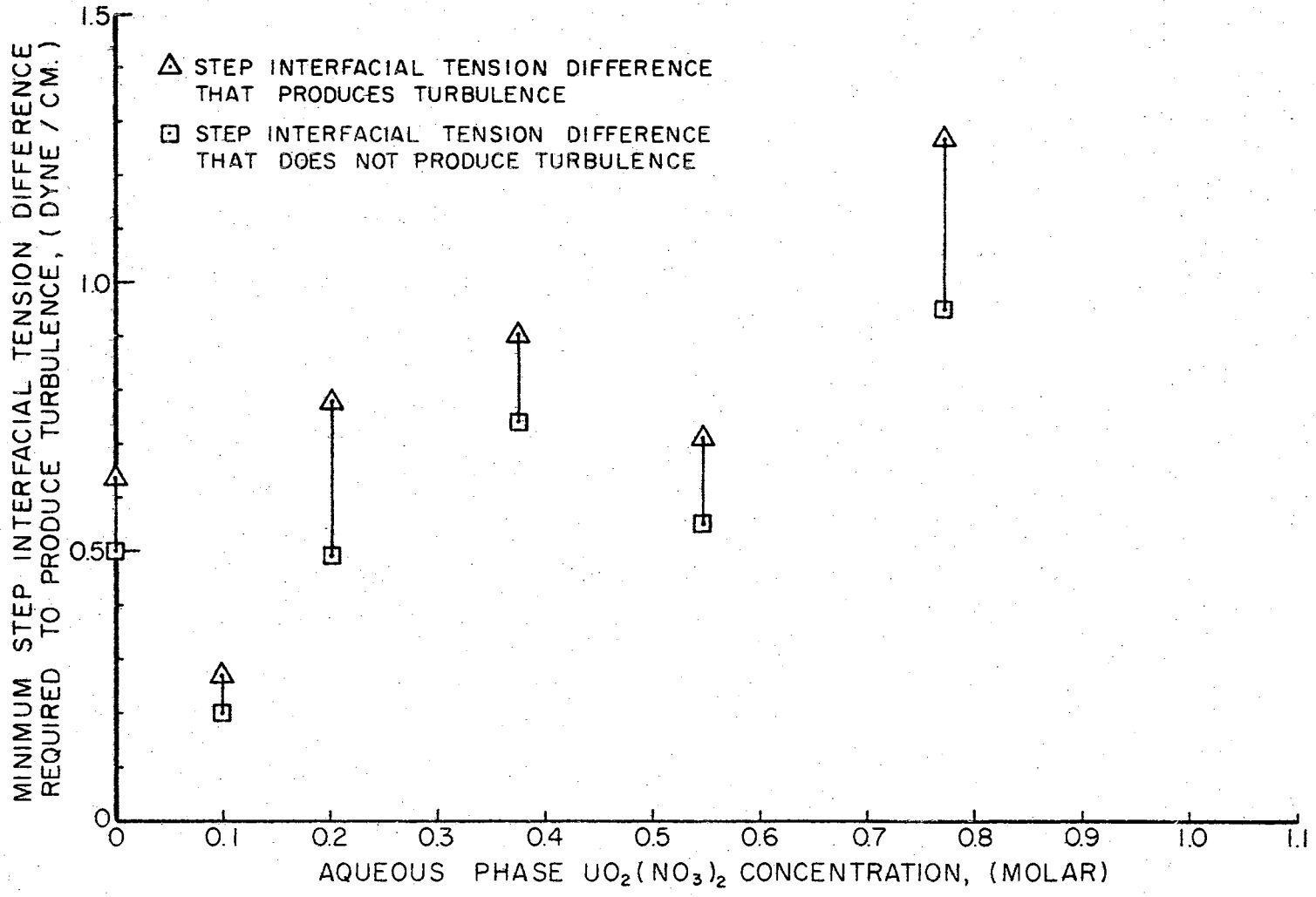

Figure 13. Step Interfacial Tension Differences Required for Turbulence

TABLE III

PHYSICAL PROPERTIES FOR AQUEOUS-ORGANIC-URANYL NITRATE SYSTEMS

System No.	Aqueous Uranyl Nitrate Conc. Producing Gradient C_o (Molar)	Diffusivity Ratio D_a/D_b	Aqueous Phase Diffusivity D_a ($cm.^2/sec.$) x 10^5	Aqueous Phase Absolute Viscosity μ_a ($Gm/cm.-sec.$) x 10^3	Aqueous Phase Kinematic Viscosity ν_a ($cm.^2/sec.$) x 10^3	Absolute Viscosity Ratio μ_a/μ_b	Kinematic Viscosity Ratio ν_a/ν_b	Distribution Coefficient Ratio of Conc. C_b/C_a	Concentration Coefficient of Interfacial Tension ζ_a (dynes/cm.-molar)
1	0.07008	2.661	0.495	9.325	9.124	0.515	0.395	0.314	7.635
	0.0897	2.591	0.482	9.403	9.138	0.498	0.384	0.580	8.346
2	0.1206	2.559	0.476	9.531	9.182	0.469	0.366	0.854	8.751
	0.1311	2.565	0.477	9.576	9.190	0.462	0.361	0.885	9.081
3	0.2422	2.839	0.528	10.101	9.379	0.412	0.326	0.941	13.776
	0.2615	2.909	0.541	10.201	9.419	0.407	0.322	0.933	14.656
4	0.4141	3.527	0.656	11.082	9.790	0.392	0.306	0.785	16.969
	0.4243	3.565	0.663	11.147	9.821	0.391	0.305	0.775	15.673
5	0.6017	4.102	0.763	12.390	10.403	0.404	0.306	0.632	9.531
	0.6197	4.269	0.794	12.529	10.467	0.405	0.306	0.621	9.021
6	0.9466	4.968	0.924	15.438	11.866	0.460	0.326	0.466	4.738
	1.0270	5.043	0.938	16.268	12.259	0.479	0.334	0.438	4.094

interfacial tension in place of an arbitrary value of unity selected by Marsh for these properties.

The computed results to Equation 1 for each of the uranyl nitrate systems tested are presented in Table IV. A plot of the disturbance factor versus aqueous phase uranyl nitrate concentration is presented in Figure 14. This plot is to aid in comparing the size of the disturbance factor for which interfacial turbulence was observed to the disturbance factor for which interfacial turbulence was not observed. The comparison of the disturbance factors and not their absolute value is of importance here, since the derivation of Marsh, Sleicher, and Heideger's theory was for a two-dimensional case and included restrictions such as a nonflexible interface which imposes increased stability on the system. Each disturbance presented is calculated at the wavelength that is the most unstable for a given system. Therefore, the disturbance factor presented represents the greatest instability of the given system.

According to Marsh, Sleicher, and Heideger's theory, all systems for which the disturbance factor and the coefficient of interfacial tension are positive should experience either stationary instability (for $D_A/D_B > 1.05$) or oscillatory instability (for $D_A/D_B < 0.95$). All systems for which the disturbance factor is negative are supposed to be stable. Also, stable systems are predicted when the value for D_A/D_B is between 0.95 and 1.05. In evaluating the results obtained in this study, Table V and Figure 14, it is concluded that all of the systems should experience stationary instability. However, as was stated previously, the absolute value of the disturbance factor should not be considered.

TABLE IV

DISTURBANCE FACTORS AND WAVE NUMBERS FOR AQUEOUS-

ORGANIC-URANYL NITRATE SYSTEMS

System No.	System Experiencing Interfacial Turbulence	Conc. Coeff. of Interfacial Tension dynes/cm.-molar	Real Value of Disturbance Factor $sec.^{-1}$	Imaginary Value of Disturbance Factor $sec.^{-1}$	Wave Number $cm.^{-1}$
1	No	6.543	4.81×10^2	1.48×10^3	-1.12×10^4
	Yes	7.839	1.28×10^2	3.95×10^2	-5.72×10^3
2	No	9.808	1.47×10^3	4.52×10^3	-1.97×10^4
	Yes	10.354	1.16×10^3	3.57×10^3	-1.75×10^3
3	No	19.032	1.30×10^4	3.94×10^4	-5.61×10^4
	Yes	19.557	1.01×10^4	3.24×10^4	-5.14×10^4
4	No	12.437	3.01×10^4	9.10×10^4	-8.01×10^4
	Yes	11.983	3.44×10^4	1.04×10^5	-8.57×10^4
5	No	7.549	1.44×10^4	4.13×10^4	-5.08×10^4
	Yes	7.288	1.58×10^4	4.56×10^4	-5.41×10^4
6	No	2.713	3.80×10^3	1.07×10^4	-2.45×10^4
	Yes	2.314	4.97×10^3	1.40×10^4	-2.82×10^4

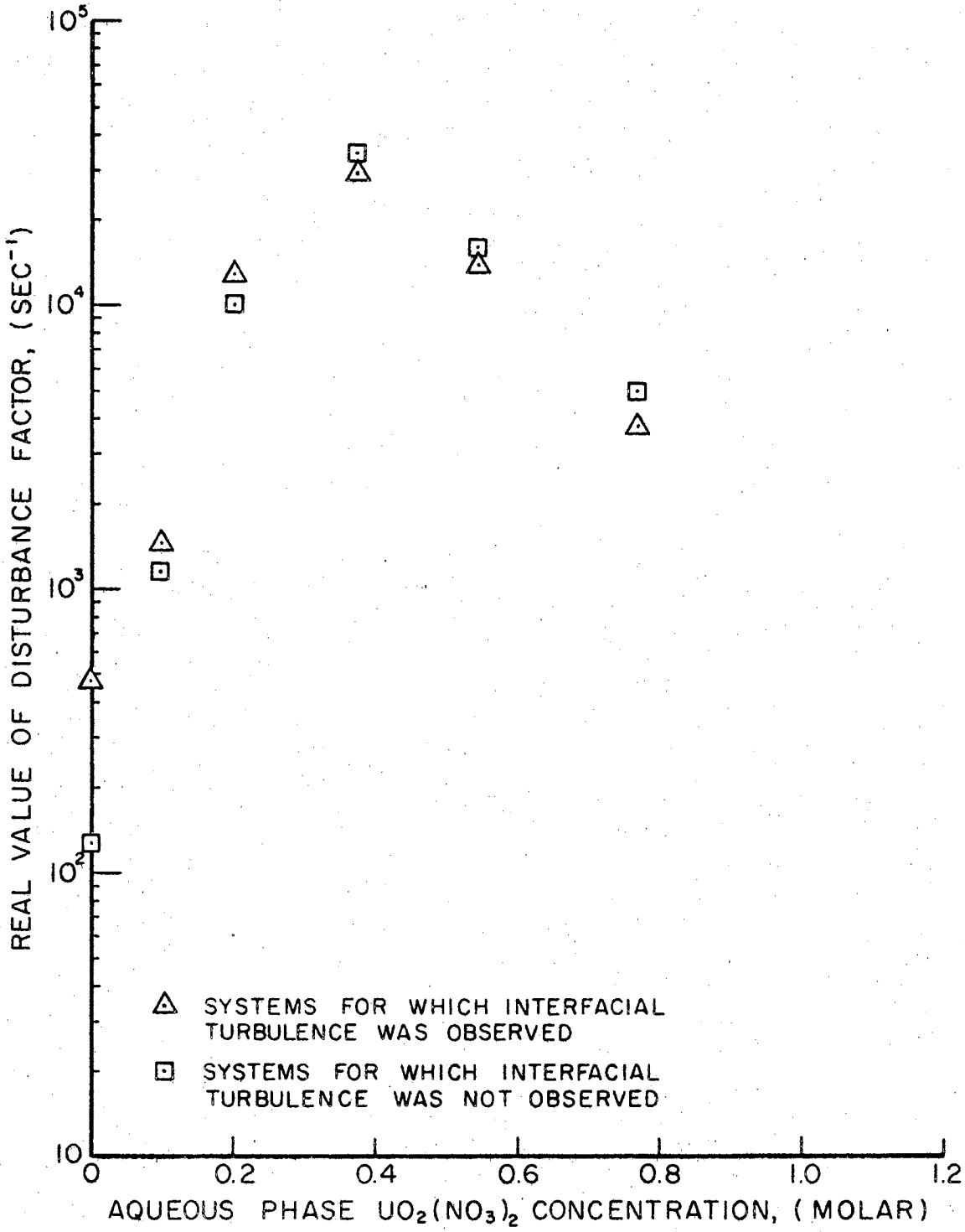

Figure 14. Disturbance Factor Required for Turbulence

TABLE V

STABILITY COMPARISON OF AQUEOUS-ORGANIC-

URANYL NITRATE SYSTEMS

System No.	Diffusivity Ratio D_A/D_B	Type of Instability (Predicted From Theory)*
1	2.661	Stationary
	2.591	Stationary
2	2.559	Stationary
	2.565	Stationary
3	2.839	Stationary
	2.909	Stationary
4	3.527	Stationary
	3.565	Stationary
5	4.102	Stationary
	4.269	Stationary
6	4.968	Stationary
	5.043	Stationary

* The theory predicts oscillatory instability for $D_A/D_B < 0.95$, stability for $0.95 \leq D_A/D_B \leq 1.05$, and stationary instability for $D_A/D_B > 1.05$ when the coefficient of interfacial tension is positive and when the solute transfer is from phase A to phase B (23).

The systems tested were compared on the basis that the greater the disturbance factor the greater the instability of the system. However, it is shown that some of the systems for which interfacial turbulence was not observed had larger disturbance factors than other systems for which interfacial turbulence was observed, Figure 14. Also, even when the two systems were at the same concentration, it is found that the disturbance factor for the system experiencing interfacial turbulence was not always greater than the disturbance factor for the system not experiencing interfacial turbulence.

It is found from Figure 14 that aqueous phase uranyl nitrate concentrations greater than 0.3754 molar had a larger disturbance factor for the systems not experiencing interfacial turbulence than for the systems experiencing interfacial turbulence. However, for aqueous phase concentrations greater than 0.3754 molar, the coefficient of interfacial tension was greater for the systems not experiencing interfacial turbulence. In all systems evaluated, the disturbance factor was always larger at a given aqueous phase uranyl nitrate concentration for systems with the larger value of the coefficient of interfacial tension. The results indicate that the disturbance factor is a stronger function of the coefficient of interfacial tension for the systems tested than of the other parameters.

This study would indicate that the disturbance factor is not sensitive enough to predict which systems will experience interfacial turbulence and which systems will not. However, the inconsistency in the disturbance factors evaluated at different concentrations might be explained by inconsistent values used for the coefficient of interfacial tension as well as other physical properties. The values for

the coefficient of interfacial tension were determined for each system by graphically constructing a tangent line to the interfacial tension curve, Figure 21, at the point of the aqueous phase uranyl nitrate concentration. This procedure for determining the coefficient of interfacial tension could lead to appreciable error. Also, since the exact uranyl nitrate concentration along the immiscible liquid-liquid interface could not be determined with the interferometer used for this study, error could result from evaluating the physical properties at the initial concentration.

CHAPTER VI

CONCLUSIONS AND RECOMMENDATIONS

A concentration gradient of solute along the interface between two immiscible liquids can be produced if the immiscible liquid interface is concave away from a very steep solute concentration gradient. This produces an interfacial tension gradient along the immiscible liquid interface which can be increased to a degree that will produce interfacial turbulence.

In order to determine the effects of interfacial tension on interfacial turbulence, it is necessary to minimize density instability in the systems studied. Therefore, it was concluded from this work that for a given system the solute can be transferred in only one direction if density stability is to be maintained.

From the study of interfacial turbulence in TBP-n-heptane-uranyl nitrate-water systems, a minimum step concentration difference was found for each concentration level below which interfacial turbulence was not produced. Therefore, it is concluded that a minimum step interfacial tension difference along the immiscible liquid interface does exist below which interfacial turbulence will not be produced. Also, it was concluded that the minimum step interfacial tension difference is nearly constant for all levels of uranyl nitrate concentration within experimental error and error in interfacial tension data. The minimum step interfacial tension difference is

believed to be a function of both interfacial tension and bulk viscosity; and, therefore, the minimum interfacial tension gradient required to produce turbulence would vary from system to system. However, the effects of viscosity were not considered in this study so no attempt was made to show a direct relation of viscosity on turbulence formation.

In evaluation of the data with regard to the theory proposed by Sternling and Scriven (39) and extended by Marsh, Sleicher, and Heideger (23), it is concluded that the systems of TBP-n-heptane-uranyl nitrate-water are all unstable only to stationary instabilities since the ratio of D_A/D_B for each system is much greater than one.

The disturbance factors, calculated from Equation 1, were found to be positive for the systems with a minimum concentration gradient required to produce turbulence as well as for the systems with a maximum concentration gradient not producing turbulence. Therefore, it would be concluded from Marsh, Sleicher, and Heideger's theory (23) that each of the systems could experience interfacial turbulence. Further comparisons were made of the disturbance factor for systems experiencing turbulence to those for systems not experiencing turbulence. It was found that some of the disturbance factors for systems in which turbulence was not observed were larger than those for systems in which turbulence was observed (even of the same aqueous and organic phase concentrations). Therefore, it is concluded that a better evaluation of the physical parameters included in the equation as well as additional parameters are needed in order for the disturbance factor method to be able to distinguish the systems for which turbulence can be observed from those for which turbulence cannot be

observed.

Recommendations for the continuation of this study of interfacial turbulence are listed and discussed below:

1. The optical system should be modified in order that the concentration gradient required to produce turbulence along the immiscible liquid-liquid interface can be measured. This might be accomplished by enlarging the light beam magnification prior to transmitting it through the first Savart plate. Also, the first and possibly the second Savart plates should be exchanged for thinner plates.
2. The cell image should be enlarged before being photographed, but it is believed necessary that the entire immiscible liquid-liquid interface be viewed since turbulence might occur at any position along the interface.
3. The cell chamber should be made thinner in the direction of the optical path. This would aid in measuring large concentration gradients and also eliminate part of the confusion caused by uneven turbulence.
4. The study of turbulence produced in a drop should be considered. This would allow a large interfacial concentration gradient to be formed. However, no concentration measurements could be made within the drop.
5. More accurate physical property data should be obtained for the systems to be studied. This would include viscosity, distribution, diffusivity, and interfacial tension data.
6. The temperature as well as the concentration effect should be considered. The systems should be run at different

constant temperatures which would allow the viscosity of the systems to be changed without changing the concentration.

7. A study should be made of the temperature gradient along the immiscible liquid-liquid interface required to produce turbulence. This would allow one to determine which effect played the major role in producing interfacial turbulence--the heat of reaction caused by mass transfer or the concentration gradient along the interface. There have been conflicting theories along these lines by Haydon (16) and Lewis (21).

   The birefringent interferometer with slight modifications of the optical system can be used to measure the temperature gradients along the immiscible interface.

8. Different or additional systems should be considered in order to study both oscillatory and stationary instability.

A SELECTED BIBLIOGRAPHY

1. Berg, J. C. and A. Acrivos. Chem. Eng. Sci., 20 (1965), 737.

2. Block, M. J. Nature (London), 178 (1956), 650.

3. Bryngdahl, O. Journal of the Optical Society in America, 53, No. 5 (1963), 571.

4. Bryngdahl, O. and S. Ljunggren. J. Phys. Chem., 64 (1960), 1264.

5. Burger, L. L. U. S. Atomic Energy Commission Document. HW-62087 (1959).

6. Bush, D. E. "Effect of Concentration Difference on the Rates of Transfer of Uranyl Nitrate Between Water and TBP." (unpub. Ph.D. thesis, Oklahoma State University, 1966).

7. Davies, T. V. and D. A. Haydon. Proc. Roy. Soc. (London), A243 (1958), 492.

8. Dorotan, A. Private communication, Oklahoma State University, Stillwater, Oklahoma.

9. Drew, T. B., J. W. Hoopes, Jr. and T. Vermeulen. Advances in Chemical Engineering. New York: Academic Press, 1966, pp. 61-123.

10. Edmison, M. T. "Safety Considerations for the Use of Lasers." (Department of Physics, Oklahoma State University, November, 1965).

11. Finley, J. B. "Diffusion in Concentrated Uranyl Nitrate Solutions." (unpub. Ph.D. thesis, Oklahoma State University, 1964).

12. Garner, F. H., C. W. Nutt and M. F. Mohtadi. Nature (London), 175 (1955), 603.

13. Gore, R. W. "An Optical Study of Interfacial Turbulence." Preprint 36, Presented at Technical Session No. 10, Fifty-fourth Annual Meeting, New York, New York, December 2-7, 1961, American Institute of Chemical Engineers, 345 East 47 Street, New York 17, New York.

14. Hahn, H. T. U. S. Atomic Energy Commission Document. HW-32626 (1954).

15. Haydon, D. A. Nature (London), 176 (1955), 839.

16. Haydon, D. A. Proc. Roy. Soc. (London), A243 (1958), 483.

17. Jeffreys, H. Phil. Mag., 2 (1926), 833.

18. Langmuir, I. and D. B. Langmuir. J. Phys. Chem., 31 (1927), 1719.

19. Lewis, J. B. Chem. Eng. Sci., 3 (1954), 248.

20. Lewis, J. B. Chem. Eng. Sci., 8 (1958), 295.

21. Lewis, J. B. and H. R. C. Pratt. Nature (London), 171 (1953), 1155.

22. Mansfield, W. W. Australian J. Scientific Research, 5A (1952), 331.

23. Marsh, B. D., C. A. Sleicher, Jr., and W. J. Heideger. "Marangoni Instability With Time-Dependent Undisturbed State." Presented at Fifty-eighth Annual Meeting, December, 1965, American Institute of Chemical Engineers, 345 East 47 Street, New York 17, New York.

24. McBain, J. W. and T. M. Woo. Proc. Roy. Soc. (London), A163 (1937), 182.

25. Neurath, H. Chem. Revs., 30 (1942), 357.

26. Nield, D. A. J. Fluid Mech., 19 (1964), 341.

27. Olander, D. L. and M. Benedict. Nuclear Science and Eng., 15 (1963), 354.

28. Orell, A. and J. W. Westwater. A.I.Ch.E. J., 8, No. 3 (1962), 350.

29. Pearson, J. R. A. J. Fluid Mech., 4 (1958), 489.

30. Pellew, A. and R. V. Southwell. Proc. Roy. Sci. (London), A176 (1940), 312.

31. Rukenshtein, E. International Chem. Eng., 5 (1965), 88.

32. Sani, R. L. A.I.Ch.E. J., 11, No. 6 (1965), 971.

33. Scriven, L. E. Chem. Eng. Sci., 12 (1960), 98.

34. Scriven, L. E. and C. V. Sternling. J. Fluid Mech., 19 (1964), 321.

35. Scriven, L. E. and C. V. Sternling. Nature (London), 187 (1960), 186.

36. Sherwood, T. K. and J. C. Wei. Ind. Eng. Chem., 49 (1957), 1030.

37. Shoemaker, D. P. and C. W. Garland. Experiments in Physical Chemistry. New York: McGraw-Hill Book Company, Inc., 1962, pp. 438-439.

38. Skinner, R. D. "A Birefringent Interferometer for Diffusion Measurements." (unpub. M.S. thesis, Oklahoma State University, 1964).

39. Sternling, C. V. and L. E. Scriven. A.I.Ch.E. J., 5 (1959), 514.

40. Strong, J. Concepts of Classical Optics. San Francisco and London: W. H. Freeman and Company, 1958, pp. 400-409.

41. Svensson, H. Optica Acta, 1 (1954), 25.

42. Thornton and Pratt. Trans. Instn. Chem. Engrs., 31 (1953), 292.

43. Ward, F. H. and L. H. Brooks. Trans. Faraday Soc., 48 (1952), 1124.

A P P E N D I X A

APPENDIX A

ALIGNMENT PROCEDURE

The optical system of the interferometer was aligned using an alignment telescope, Figure 8, page 37. The alignment telescope was positioned at one end of the optical bench using the following procedure: The base of the alignment telescope was leveled by three leveling screws. The telescope was adjusted to the desired height and aligned with the center of the optical bench. Alignment of the telescope with the center of the optical bench was accomplished by aligning the cross-hairs of the telescope with a copper wire hanging in the center at each end of the optical bench. The telescope was then leveled with the aid of a leveling bubble attached to the telescope.

The constant temperature water bath was bolted onto the optical bench six feet from the end of the bench opposite the alignment telescope. The optical flat windows were then aligned with the center of the optical bench using the telescope.

The laser was positioned at the end of the optical bench opposite the telescope. Alignment of the laser was accomplished by centering the output end of the laser tube with the telescope. This was done with the laser light turned off, since the light rays from the laser are harmful when viewed directly (10). The light beam from the laser was then centered with the optical bench by the following procedure:

A cross mark on a piece of translucent paper was positioned in the center of the optical bench, opposite the laser, using the telescope. The laser was turned on, and the collimated light beam from the laser was centered with the cross mark on the translucent paper by tilting the laser.

The optical flat windows of the constant temperature bath and the interfacial turbulence cell were aligned using the laser. The optical flat windows in the constant temperature water bath were aligned one at a time by the following procedure: The optical flat was tilted, using the three adjusting screws attached to the window, until the surface of the flat was normal to the light beam from the laser. The surface of the optical flat is normal to the light beam when the light beam is reflected directly into the light source. The two optical flats of the cell were aligned together since there was no separate adjustment for the flats. However, the sides of the cell were ground parallel to one-ten-thousandth of an inch so that the cell could be aligned as a unit. The cell was mounted onto the constant temperature bath with the center of the cell in the center of the optical path. The cell was independently realigned each time after it had been removed from the bath.

After the optical flats had been aligned, the rest of the optical components were aligned in order, from the laser to the camera. The lenses were aligned by centering each lens with the cross-hair of the telescope. Then the light beam through each lens was centered with a cross mark, placed on a piece of translucent graph paper, that had been centered several feet in front of the lens. The Savart plates and polarizers were aligned by centering them with the cross-hair of

the telescope and then adjusting them until a light beam from the Gauss eyepiece of the telescope was reflected directly into the telescope. This placed the Savart plates and the polarizers in the center of the optical axis with the surfaces of each plate normal to the optical axis.

The camera was aligned by focusing the camera lens on a plane through the interfacial turbulence cell. The plane was located one-third of the cell thickness from the optical flat near the camera. The camera lens focusing was accomplished by forming a sharp interface between two solutions of different concentrations in the cell chamber and then adjusting the camera until a sharp fringe pattern was observed in the viewer of the camera. The fringe pattern should be symmetric about the horizontal interface when the camera is in correct focus.

The calculation of the lens spacing used in the major part of this work is presented with the aid of Figure 15. The equation used to determine the position of each lens is

$$1/f = 1/p + 1/q \qquad \text{(A-1)}$$

where f is the focal length of the lens, p is the object distance from the lens, and q is the image distance from the lens. The equation used to determine the magnification of the lens system is

$$I_L/O_L = I_D/O_D \qquad \text{(A-2)}$$

where I_L and O_L are the image and object size, respectively, and I_D and O_D are the image and object distance from the lens, respectively. Both of these equations can be found in most standard physics

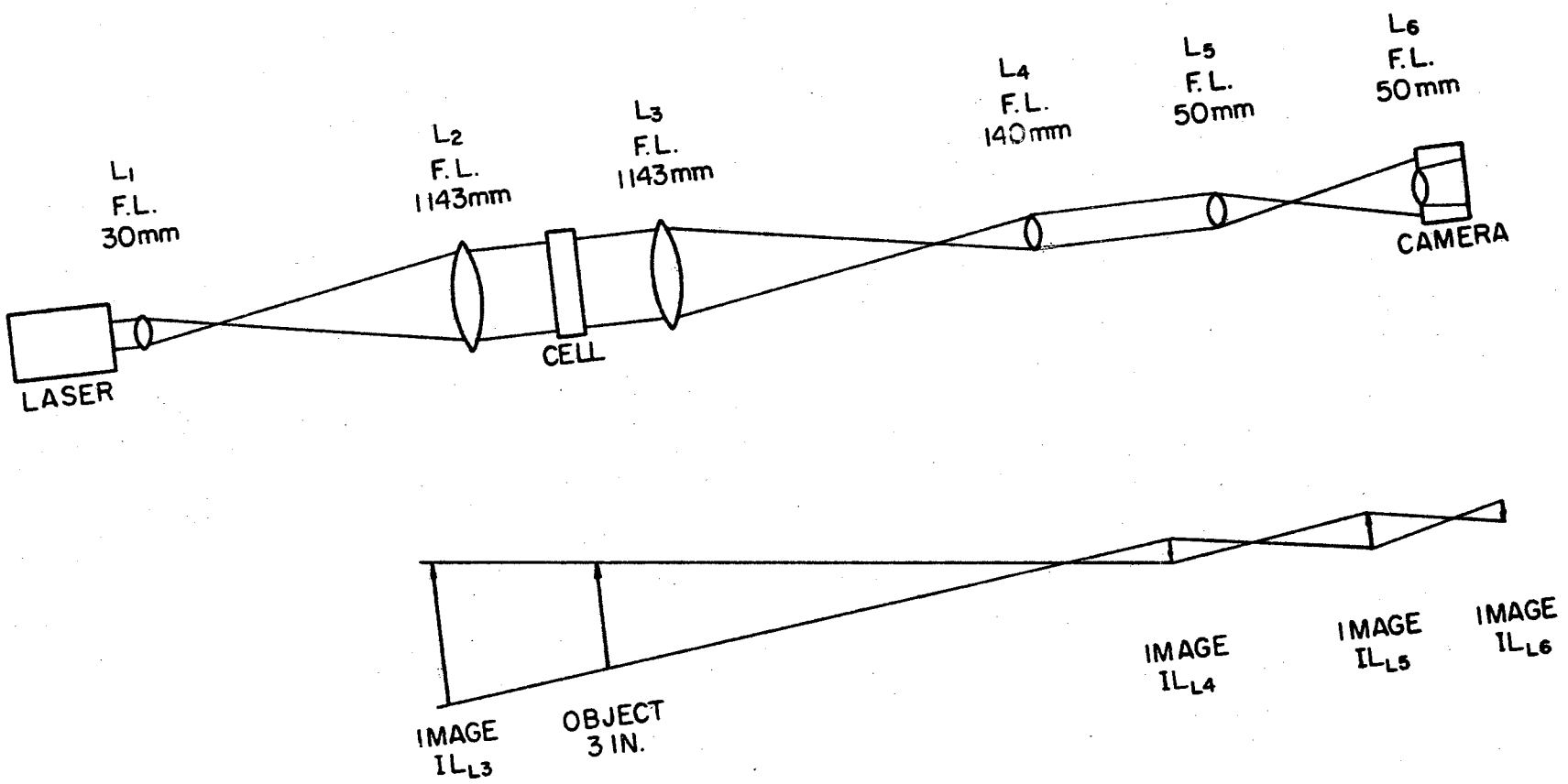

Figure 15. Diagram of Lens System

textbooks.

Lenses L_1 and L_2 are separated by the focal length of L_1 plus the focal length of L_2, in this case 1,173 mm. This produces a collimated light beam about 2.21 inches in diameter that passes through the cell.

Using Equation A-1 and the focal length of each lens from Figure 15, the lens spacing is determined. When a negative value for q is obtained, the image is located on the same side of the lens as the object. For lens L_3 placed 355 mm. to the right of the cell

$$1/1,143 \text{ mm.} = 1/355 \text{ mm.} + 1/q$$

$$q = -514.9 \text{ mm.}$$

The image plane for lens L_3 then becomes the object plane for L_4. But, lenses L_3 and L_4 must be separated by a distance, the focal length of L_3 plus the focal length of L_4, of 1,283 mm. in order that collimated light rays will be transmitted from L_4. For this spacing

$$1/140 \text{ mm.} = 1/1797.9 \text{ mm.} + 1/q$$

$$q = 151.8 \text{ mm.}$$

The spacing of lens L_5 is critical in producing magnification and in controlling light intensity on the film. For this work, lens L_5 was placed 245 mm. to the right of lens L_4. Therefore,

$$1/50 \text{ mm.} = 1/93.2 \text{ mm.} + 1/q$$

$$q = 107.9 \text{ mm.}$$

For the spacing of the camera lens, an extension tube was used in order to increase magnification. Therefore, the image distance,

q = 90 mm., for this lens was set so that

$$1/50 \text{ mm.} = 1/p + 1/90 \text{ mm.}$$

$$p = 112.5 \text{ mm.}$$

The camera lens is thus placed 220.4 mm. to the right of lens L_5. This is the sum of the image distance from lens L_5 plus the object distance from the camera lens L_6.

The magnification for the above lens spacing can now be calculated using Equation A-2. The cell chamber is assumed to be three inches in length for purposes of these calculations. The length of the cell image from lens L_3 is IL_{L3}.

$$IL_{L3}/3 \text{ in.} = -514.9 \text{ mm.}/355 \text{ mm.}$$

$$IL_{L3} = 4.35 \text{ in.}$$

The image IL_{L3} is located in a plane 149.9 mm. to the left of the cell and is in an upright position.

The length of the cell image from lens L_4 is IL_{L4}.

$$IL_{L4}/4.35 \text{ in.} = 151.8 \text{ mm.}/1797.9 \text{ mm.}$$

$$IL_{L4} = 0.37 \text{ in.}$$

The image IL_{L4} is located in a plane 151.8 mm. to the right of lens L_4 and in an inverted position.

The length of the cell image from lens L_5 is IL_{L5}.

$$IL_{L5}/0.37 \text{ in.} = 107.9 \text{ mm.}/93.2 \text{ mm.}$$

$$IL_{L5} = 0.43 \text{ in.}$$

The image IL_{L5} is located in a plane 97.9 mm. to the right of lens L_5 and in an upright position.

The length of the cell image on the film is IL_{L6}.

$$IL_{L6}/0.43 \text{ in.} = 100 \text{ mm.}/112.5 \text{ mm.}$$

$$IL_{L6} = 0.38 \text{ in.}$$

The inverted image IL_{L6} is located in the same plane as the film. The magnification of the cell image on the film as calculated by the above procedure is approximate due to error in positioning the lenses. Therefore, these calculations are used only to determine the desired position of the lenses. The actual magnification of the cell image was determined following a procedure detailed in Appendix D.

A P P E N D I X B

APPENDIX B

CELL CLEANING PROCEDURE

The cell chamber, feed lines, and solution tanks were cleaned after each run. The cleaning procedure was started following the draining of the system after each run. While the cell was still in the constant temperature bath with the discharge and feed lines connected, the cell chamber, feed lines, and solution tanks were flushed several times with large volumes of distilled water (about 250 milliliters per flush). When uranyl nitrate solutions had been used, a slightly different rinse procedure was followed to eliminate the collection of large volumes of waste. Each solution tank and line was rinsed with a small volume of distilled water squirted around the edges of the tank from a squeeze bottle. The cell was then removed from the constant temperature bath and the cell chamber rinsed four times with about 20 milliliters of distilled water for each rinse. The rinse water was collected and stored in bottles labeled radioactive waste.

After thorough rinsing of the cell chamber, the cell was partially disassembled by removing both optical flats and glass interliners. The cell chamber and connection lines were then blown dry with dry compressed air. A piece of 0.006 inch shimstock was forced through each slot at the center of the cell to remove any particles that may have been collected.

The solution tanks and feed lines were rinsed with acetone, distilled water and blown dry with compressed dry air.

Preparation of Optical Flats and Glass Cell Liners

The optical flats and one set of glass cell liners were coated with General Electric Silicones Dri-film SC-87 to prevent their surfaces from being water wet. A second set of glass cell liners was cleaned with sulfuric acid so that their surfaces would be completely water wet. The cell liners which were water wet would produce an interface between the aqueous and organic phase concave about the organic phase, while the other liners would produce an interface concave about the water phase.

The optical flats required further preparation since a 90° angle between the organic-aqueous interface and the optical flats must be maintained. The optical flats, after being coated with Dri-film SC-87 and allowed to dry for about 24 hours, were polished with jeweler's rouge to remove enough dri-film so that the surface was partially water wet thus permitting a 90° angle to be formed between the organic-aqueous interface and the optical flat. This process was accomplished by trial and error with successive polishing and testing of the surface. The optical flat was tested by dipping it into a beaker filled with equal portions of the organic and aqueous phases to be investigated. Once the surfaces had been prepared, the above procedure did not need to be repeated for several runs.

The optical flats and cell liners were cleaned following each run. This was accomplished by rinsing each surface first with acetone and then distilled water. The surfaces were then dried and polished

with Kimwipes. The optical flats and cell liners were handled with clean rubber gloves to prevent their surfaces from being contaminated with oil from the skin.

Assembly of the Cell

The glass liners were placed in the cell chamber under the stainless steel flaps which hold the liners tight against the cell walls. The optical flats were then affixed to the cell with teflon gaskets ten microns thick between the flats and the stainless steel cell surface. Each flat was tightened firmly (but not excessively) with the four press screws to prevent leaks.

The cell was placed back into the constant temperature bath with the feed and discharge lines appropriately attached for the desired flow. The cell was then aligned and made ready for the next run.

A P P E N D I X C

APPENDIX C

EQUATIONS FOR DETERMINING DIFFUSION COEFFICIENTS

Equations for determining diffusion coefficients from measurements obtained using the birefringent interferometer are derived as follows: Fick's second law of diffusion is used, assuming the diffusion coefficient D is constant and considering only one direction of transfer.

$$\frac{\partial C}{\partial t} = D \frac{\partial^2 C}{\partial X^2} \qquad \text{(C-1)}$$

The boundary conditions are

$$C\ (X,\ 0) = 0 \text{ for } X > 0$$

and

$$C\ (X,\ 0) = C_o \text{ for } X < 0$$

X = 0 is the center of the cell chamber where an infinitely sharp interface is formed at time equal zero. From Hans Neurath (24), the concentration as a function of the position in the cell is given by Equation C-2.

$$C_x = \frac{C_o}{2}\left(1 - \frac{2}{\sqrt{\pi}} \int_o^{\frac{x}{\sqrt{4Dt}}} e^{-\frac{x^2}{4Dt}} \frac{dx}{\sqrt{4Dt}}\right) \qquad \text{(C-2)}$$

From the derivative of C_x with respect to x, Equation C-3 is obtained.

$$\frac{dC_x}{dx} = - \frac{C_o}{\sqrt{4\pi Dt}} e^{- \frac{x^2}{4Dt}} \qquad \text{(C-3)}$$

Figure 16 represents the curvature of a fringe caused by a concentration gradient within the cell at some time greater than zero.

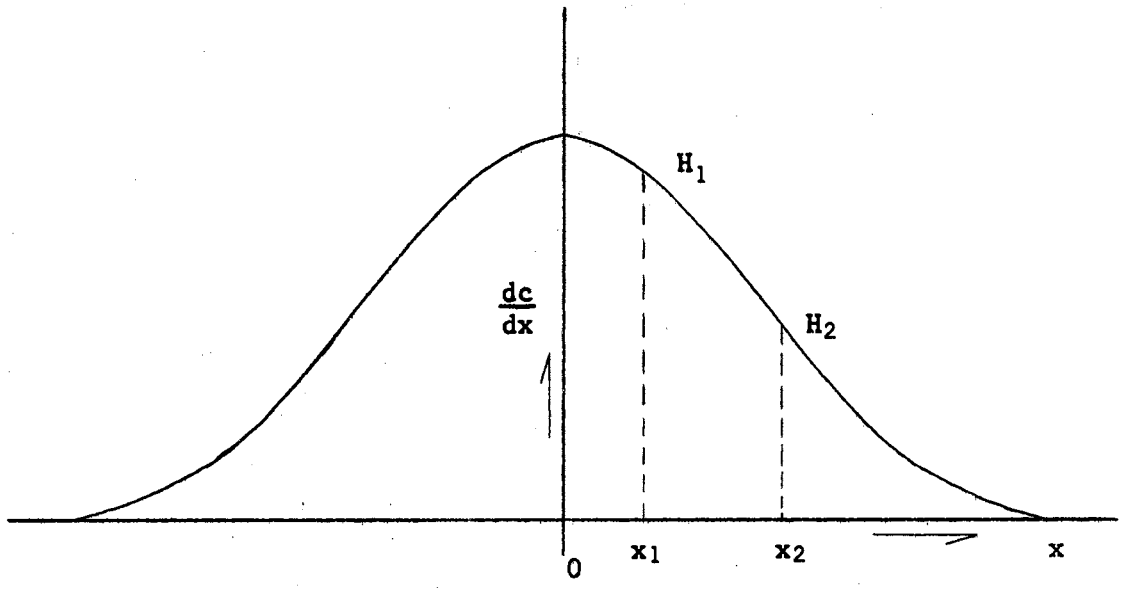

Figure 16. Plot of Concentration Gradient as a Function of Position in Cell Chamber at Time t_1

Equations C-4 and C-5 are obtained by substituting values for H_1, X_1, and H_2, X_2 into Equation C-3 where H_1 and H_2 are proportional to the value of $(dC_x/dx)_1$ and $(dC_x/dx)_2$, respectively. Let

$$AH_1 = \left(\frac{\partial C_x}{\partial x} \right)_1 = - \frac{C_o}{\sqrt{4\pi Dt}} e^{- \frac{x_1^2}{4Dt}} \qquad \text{(C-4)}$$

and

$$AH_2 = \left(\frac{\partial C_x}{\partial x} \right)_2 = - \frac{C_o}{\sqrt{4\pi Dt}} e^{- \frac{x_2^2}{4Dt}} \qquad \text{(C-5)}$$

where A is a proportionality constant. Therefore, by rearranging Equations C-4 and C-5, Equations C-6 and C-7 are obtained.

$$\frac{AH_1\sqrt{4\pi Dt}}{C_o} = -e^{-\frac{x_1^2}{4Dt}} \tag{C-6}$$

$$\frac{AH_2\sqrt{4\pi Dt}}{C_o} = -e^{-\frac{x_2^2}{4Dt}} \tag{C-7}$$

Dividing Equation C-6 by $1/H_1$ and Equation C-7 by $1/H_2$ gives

$$\frac{A\sqrt{4\pi Dt}}{C_o} = -\frac{1}{H_1}e^{-\frac{x_1^2}{4Dt}} \tag{C-8}$$

and

$$\frac{A\sqrt{4\pi Dt}}{C_o} = -\frac{1}{H_2}e^{-\frac{x_2^2}{4Dt}} \tag{C-9}$$

Equations C-8 and C-9 are combined by equating the

$$\frac{A\sqrt{4\pi Dt}}{C_o}$$

term of each.

$$\frac{1}{H_1}e^{-\frac{x_1^2}{4Dt}} = \frac{1}{H_2}e^{-\frac{x_2^2}{4Dt}} \tag{C-10}$$

Equation C-10 is simplified by separating the variables.

$$\frac{H_1}{H_2} = e^{\frac{x_2^2 - x_1^2}{4Dt}} \tag{C-11}$$

Taking the logarithm of Equation C-11 gives

$$\ln\frac{H_1}{H_2} = \frac{x_2^2 - x_1^2}{4Dt} \tag{C-12}$$

The diffusion coefficient, D, is expressed in Equation C-13 as a

function of the concentration gradient measured at two positions within the cell chamber.

$$D = \frac{x_2^2 - x_1^2}{4t \ \ell n \frac{H_1}{H_2}} \tag{C-13}$$

Correction of Diffusion Coefficient for Zero Time

Since no mechanical method available can produce a perfectly sharp interface, a zero time correction is necessary to allow for the slight mixing of the solutions at the start of the run. Let

D' = corrected diffusion coefficient

and

Δt = time correction

Substituting $t + \Delta t$ for t in Equation C-13 gives an equation for the corrected diffusion coefficient, D'.

$$D' = \frac{x_2^2 - x_1^2}{4 \ (t + \Delta t) \ \ell n \frac{H_1}{H_2}} \tag{C-14}$$

where

$$\Delta t = \frac{x_2^2 - x_1^2}{4D' \ \ell n \frac{H_1}{H_2}} - t \tag{C-15}$$

For two different times, t_1 and t_2, evaluated from Equation C-14

$$\frac{(x_2^2 - x_1^2)_1}{4D_1' \ \ell n \left(\frac{H_1}{H_2}\right)_1} - t_1 = \frac{(x_2^2 - x_1^2)_2}{4D_2' \ \ell n \left(\frac{H_1}{H_2}\right)_2} - t_2 \tag{C-16}$$

where $D_1' = D_2' = D'$. Expanding Equation C-16 gives

$$(x_2^2 - x_1^2)_1 - t_1\ 4D'\ \ell n\left(\frac{H_1}{H_2}\right)_1 = (x_2^2 - x_1^2)_2\ \frac{\ell n\left(\frac{H_1}{H_2}\right)_1}{\ell n\left(\frac{H_1}{H_2}\right)_2} -$$

$$t_2\ 4D'\ \ell n\left(\frac{H_1}{H_2}\right)_1 \qquad \text{(C-17)}$$

Solving Equation C-17 for D' gives

$$D' = \frac{(x_2^2 - x_1^2)_1 - (x_2^2 - x_1^2)_2\ \frac{\ell n\ (H_1/H_2)_1}{\ell n\ (H_1/H_2)_2}}{4t_1\ \ell n\ (H_1/H_2)_1 - 4t_2\ \ell n\ (H_1/H_2)_1} \qquad \text{(C-18)}$$

The corrected diffusion coefficient D' is evaluated in Equation C-19 as a function of times t_1 and t_2 and the uncorrected diffusion coefficients calculated at times t_1 and t_2.

$$D' = \frac{1}{t_1 - t_2}(D_1t_1 - D_2t_2) \qquad \text{(C-19)}$$

Equation for Determining Concentration of Solution at Any Point in the Cell Chamber

Letting

$$a = \frac{1}{\sqrt{4Dt}}$$

and substituting into Equation C-2 gives

$$C_x = \frac{C_o}{2} - \frac{a\ C_o}{\sqrt{\pi}} \int_o^{ax} e^{-a^2x^2}\ dx \qquad \text{(C-20)}$$

From a series expansion of $e^{-a^2x^2}$, Equation C-21 is obtained.

$$e^{-a^2x^2} = 1 - a^2x^2 + \frac{a^4x^4}{2!} - \frac{a^6x^6}{3!} + \frac{a^8x^8}{4!} - \ldots \qquad \text{(C-21)}$$

The integral of $e^{-a^2x^2}$ is then evaluated for the limits of 0 to ax

using the series expansion for $e^{-a^2x^2}$.

$$\int_0^{ax} e^{-a^2x^2}\,dx = \left[x - \frac{a^2x^3}{3} + \frac{a^4x^5}{5\cdot 2!} - \frac{a^6x^7}{7\cdot 3!} + \ldots\right]_0^{ax}$$

$$= ax - \frac{a^5x^3}{3} + \frac{a^9x^5}{5\cdot 2!} - \frac{a^{13}x^7}{7\cdot 3!} + \ldots \qquad \text{(C-22)}$$

Neglecting all but the first two terms and substituting into Equation C-20 gives

$$C_x = \frac{C_o}{2} - \frac{a^2\,C_o\,x}{\sqrt{\pi}} + \frac{a^6\,C_o\,x^3}{3\sqrt{\pi}} \qquad \text{(C-23)}$$

From Equation C-13

$$a = \sqrt{\frac{\ell n\ (H_1/H_2)}{x_2^{\,2} - x_1^{\,2}}} \qquad \text{(C-24)}$$

Substituting Equation C-24 into Equation C-23 gives

$$C_x = \frac{C_o}{2} - \left[\frac{\ell n\ (H_1/H_2)}{x_2^{\,2} - x_1^{\,2}}\right]\left[\frac{C_o\,x}{\sqrt{\pi}}\right] + \left[\frac{\ell n\ (H_1/H_2)}{x_2^{\,2} - x_1^{\,2}}\right]^3\left[\frac{C_o\,x^3}{3\sqrt{\pi}}\right] \qquad \text{(C-25)}$$

Using Equation C-25, the solute concentration at any position in the cell can be calculated from a fringe pattern obtained with the birefringent interferometer described in this work.

A P P E N D I X D

APPENDIX D

EVALUATION OF INTERFACIAL TENSION GRADIENT ALONG AN INTERFACE

The equipment and evaluation procedure explained below were not used in this study because the fringe pattern, produced by the large concentration gradient required to cause interfacial turbulence, could not be measured. However, with proper modification of the interferometer, a fringe pattern can be obtained, even at large concentration gradients, from which measurements can be made.

Equipment

The interfacial tension gradient along an immiscible liquid-liquid interface is evaluated by measuring the fringe profile produced by a concentration gradient within the interfacial turbulence cell. The fringe pattern is photographed onto a 35 mm Kodak high contrast copy film (ASA2). The fringe profile is measured directly from the 35 mm film negative with a densitometer arrangement, Figure 17.

The densitometer arrangement consists of a Photovolt Corporation Model 520-M densitometer with the photoelectric cell type C connected to the viewing scope of a Gaertner Scientific Corporation, Model M2001A toolmaker's microscope. The stage of the toolmaker's microscope has micrometer heads for both longitudinal and cross motion with a tangent screw for rotating the stage about the vertical axis. The

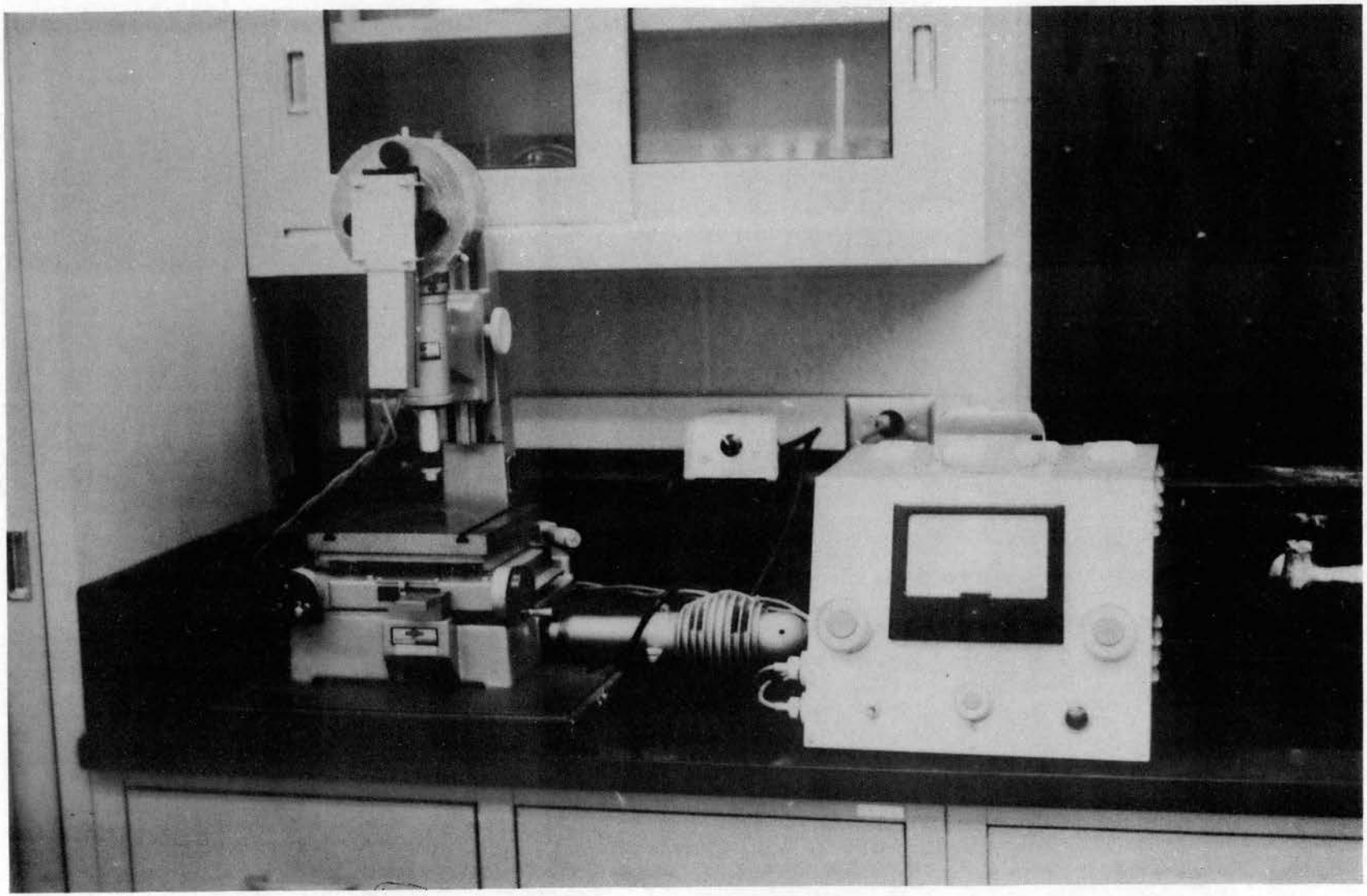

Figure 17. Densitometer Arrangement

distance traveled by the stage in both directions can be measured to ±1 micron. The microscope is illuminated by a D.C. light with adjustable voltage from 5.0 to 7.5 volts for light intensity variation. The densitometer has an ammeter with four scale ranges of 1, 10, 100, and 1,000 from which the relative film density can be determined.

Procedure

The photograph taken just before the initiation of interfacial turbulence is analyzed. The procedure for obtaining the photograph is outlined in Chapter IV. An example photograph of the concentration gradient along an immiscible liquid-liquid interface is presented in Figure 18.

Figure 19 represents a fringe pattern with which the measurement of the fringe profile will be illustrated. The fringe profile is measured using the densitometer arrangement. Three measurements, (H_1, x_1), (H_2, x_2), and (H_3, x_3), are made for each fringe as illustrated in Figure 19. H is the horizontal distance measured from the base line to the fringe displacement. x is the vertical distance from the point at which H was measured to the center line. The base line of the fringe is taken as the position for which the fringe is straight (no change in concentration gradient), and the center line of the fringe pattern is taken as the position of maximum fringe displacement (maximum change in concentration gradient, usually at the center of the cell chamber). One of the points (H_3, x_3) measured for each fringe is located at the interface h. The concentration can be calculated at several points along the interface h (detailed in Appendix C). The interfacial concentration gradient required to cause

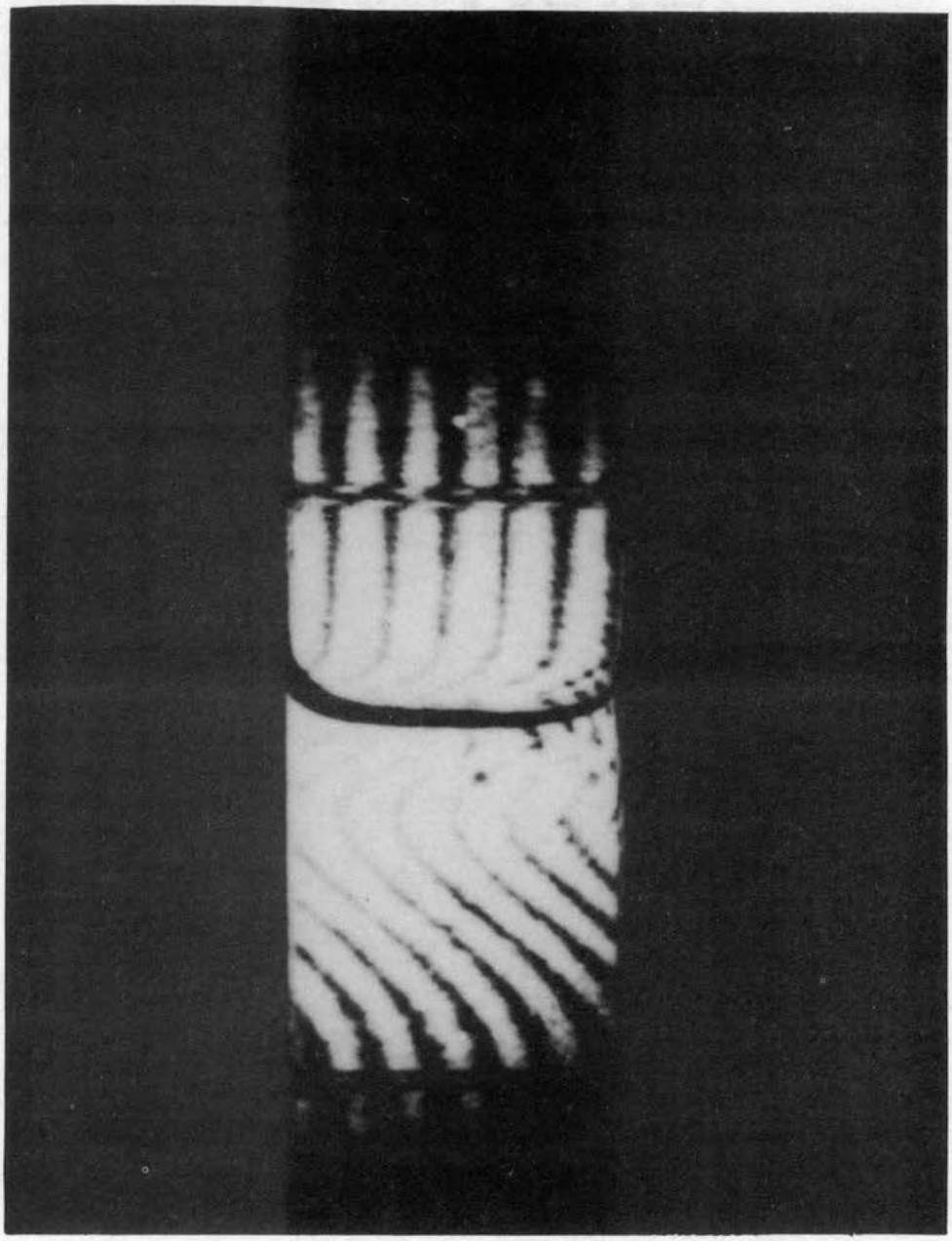

Figure 18. Photograph of Concentration Gradient in TBP-n-Heptane-Uranyl Nitrate-Water System

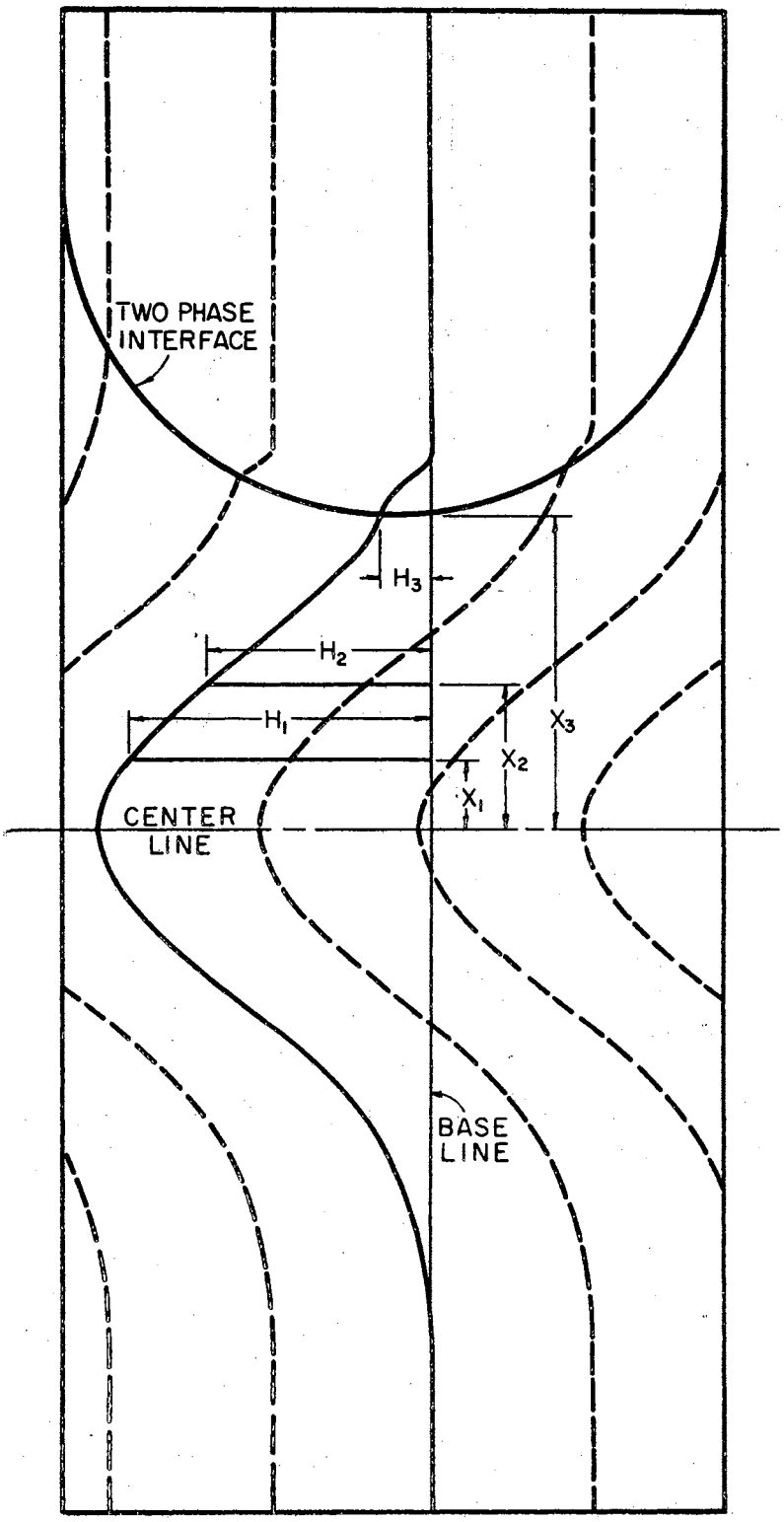

Figure 19. Diagram Representing a Fringe Pattern Caused by a Concentration Gradient

interfacial turbulence can then be determined from a plot of the concentration along the interface. Also, the interfacial tension gradient required to cause turbulence can be calculated from a concentration interfacial tension relation.

Magnification Measurements

The actual magnification of the optical system was determined by dividing the image size photographed on a 35 mm negative by the actual object size. This was accomplished by measuring the spacing of two wires placed across the face of the cell (object size) and measuring the fringe spacing caused by the wires on the 35 mm negative (image size) using the toolmaker's microscope for both measurements. Sample calculations for the magnification of the optical system used for the major part of this work are presented below.

The separation of the wires on the cell and the separation of the image of the wires on the 35 mm negative were each measured in the center since the two wires were not perfectly parallel.

Separation of Two Wires on Cell = 39199.0 microns

Separation of Wire Image on Film = 4146.5 microns

Optical System Magnification = 4146.5 microns/39199.0 microns

= 0.1058

A P P E N D I X E

APPENDIX E

PHYSICAL PROPERTIES OF SOLUTIONS

The physical properties of the pure components used in this work are presented in Table VI.

Phase Equilibrium Concentration

The organic phase concentration of uranyl nitrate in phase equilibrium with the aqueous phase is plotted as a function of the aqueous phase uranyl nitrate concentration in Figure 20. Data used to construct Figure 20 were obtained from Dorotan (8). The organic and aqueous phases were equilibrated at 77° ± 0.5°F. In determining the equilibrium distribution data, only the aqueous phase concentration was measured directly. The organic phase concentration was calculated from a material balance where the changes in volume of the aqueous and organic phases were not considered.

Interfacial Tension

The interfacial tension between the organic phase (30 percent TBP and 70 percent n-heptane) and the aqueous phase is presented as a function of the aqueous phase uranyl nitrate concentration in Figure 21. Data used to construct Figure 21 were obtained from Dorotan (8). The interfacial tension measurements were made at 25 ± 0.5°C using the pendent drop method. The average deviation in the interfacial

TABLE VI

PROPERTIES AND PURITY OF COMPONENTS USED

Acetone	
Grade	Technical
Density (gm./ml.) at 20°C	0.792
Toluene	
Grade	Fisher Certified Reagent
Density (gm./ml.) at 20°C	0.86694
Residue After Evaporation	0.0005%
Substances Darkened by H_2SO_4	P.T.
Sulfur Compounds (as S)	0.0006%
Water	0.02%
Boiling Range	110.5° - 110.8°C
n-Heptane	
Grade	Analytical Reagent
Density (g/ml.) at 25°C	0.710
Acidity (as CH_3COOH) Approx.	0.002%
Residue After Evaporation	0.001%
Sulfur Compounds (as S)	0.005%
Boiling Point	98.4°C
Boiling Point Range	4.0°C
Tributyl Phosphate	
Grade	Technical
Specific Gravity at 25°C	0.973
Boiling Point	287°C

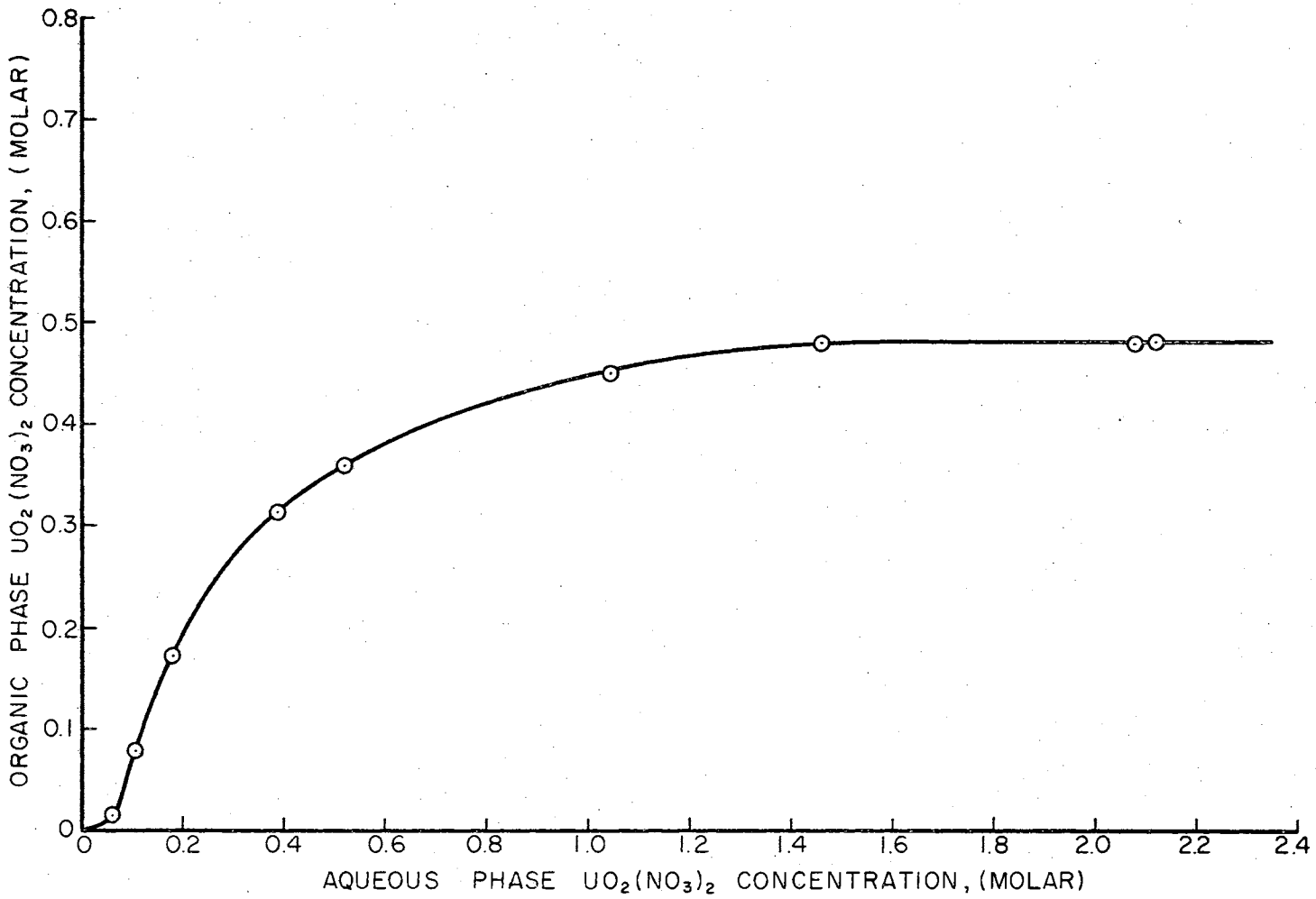

Figure 20. Equilibrium Concentration Distribution for TBP-n-Heptane-Uranyl Nitrate-Water System

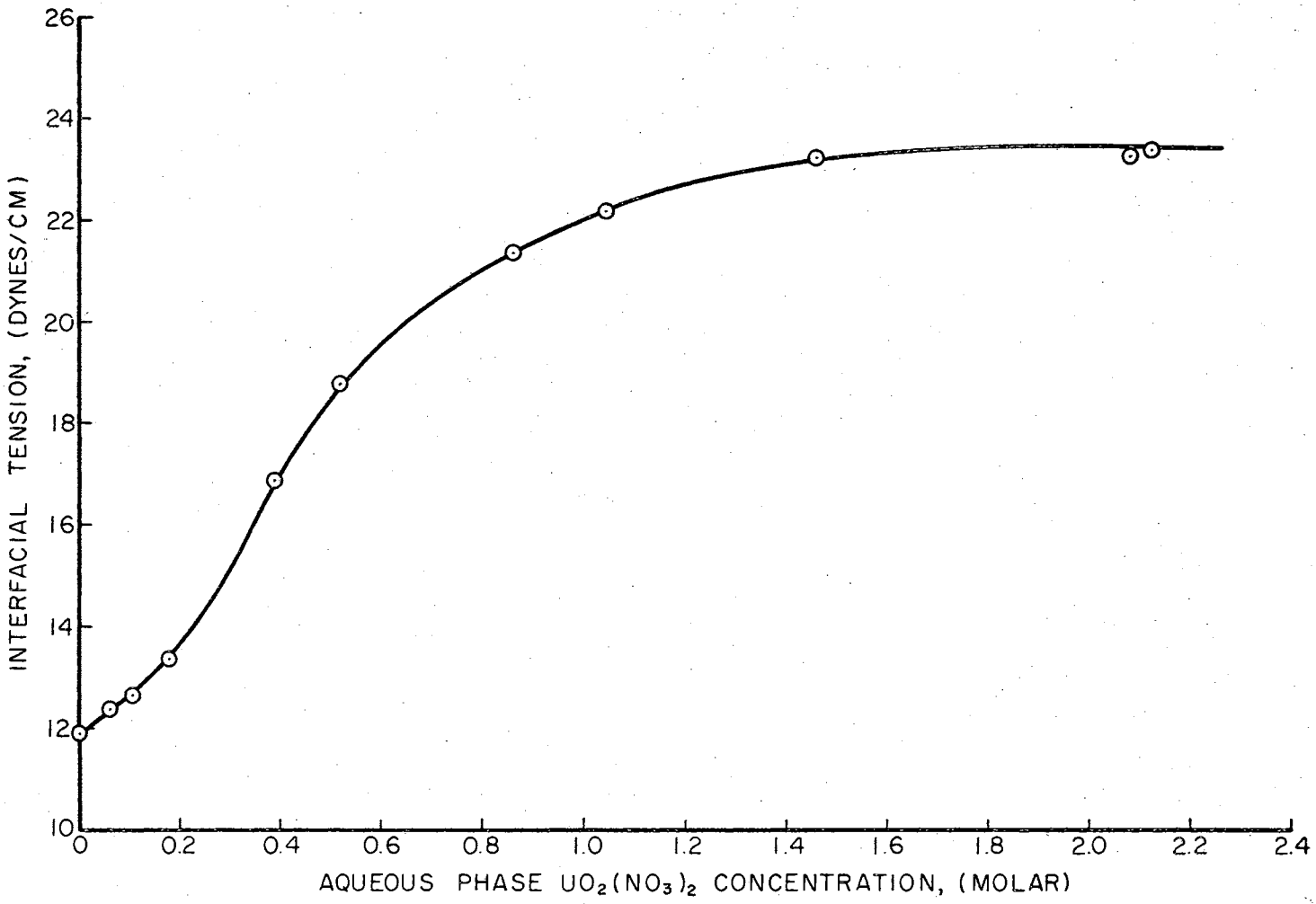

Figure 21. Interfacial Tension for TBP-n-Heptane-Uranyl Nitrate-Water System

tension measurements was found to be ±0.13 dyne/cm.

Viscosity

The viscosity of the aqueous phase as a function of uranyl nitrate concentration and the viscosity of the organic phase as a function of uranyl nitrate concentration are represented by Equations E-1 and E-2, respectively.

$$\mu_w = 9.069 + 3.411\ C_w + 3.504\ C_w^2 \qquad \text{(E-1)}$$

$$\mu_s = 17.562 + 24.08\ C_s + 27.623\ C_s^2 \qquad \text{(E-2)}$$

where viscosity is in millipoises and the concentration of uranyl nitrate in each phase is in molar concentration. Equation E-2 was derived, for an organic phase consisting of 70 percent Amsco and 30 percent TBP, by Bush (6).

Density

The density of the aqueous phase as a function of uranyl nitrate concentration is represented by Equation E-3.

$$\rho_w = 1.0 + 0.318\ C_w \qquad \text{(E-3)}$$

where density is in g/cc and the concentration of uranyl nitrate in the aqueous phase is in molar concentration. The above equation was obtained from Bush (6).

The density of the organic phase (30 percent TBP and 70 percent n-heptane) as a function of the uranyl nitrate concentration is presented in Figure 22. The data used in constructing Figure 22 were obtained from Dorotan (8). The density was measured at 77° ± 0.5°F

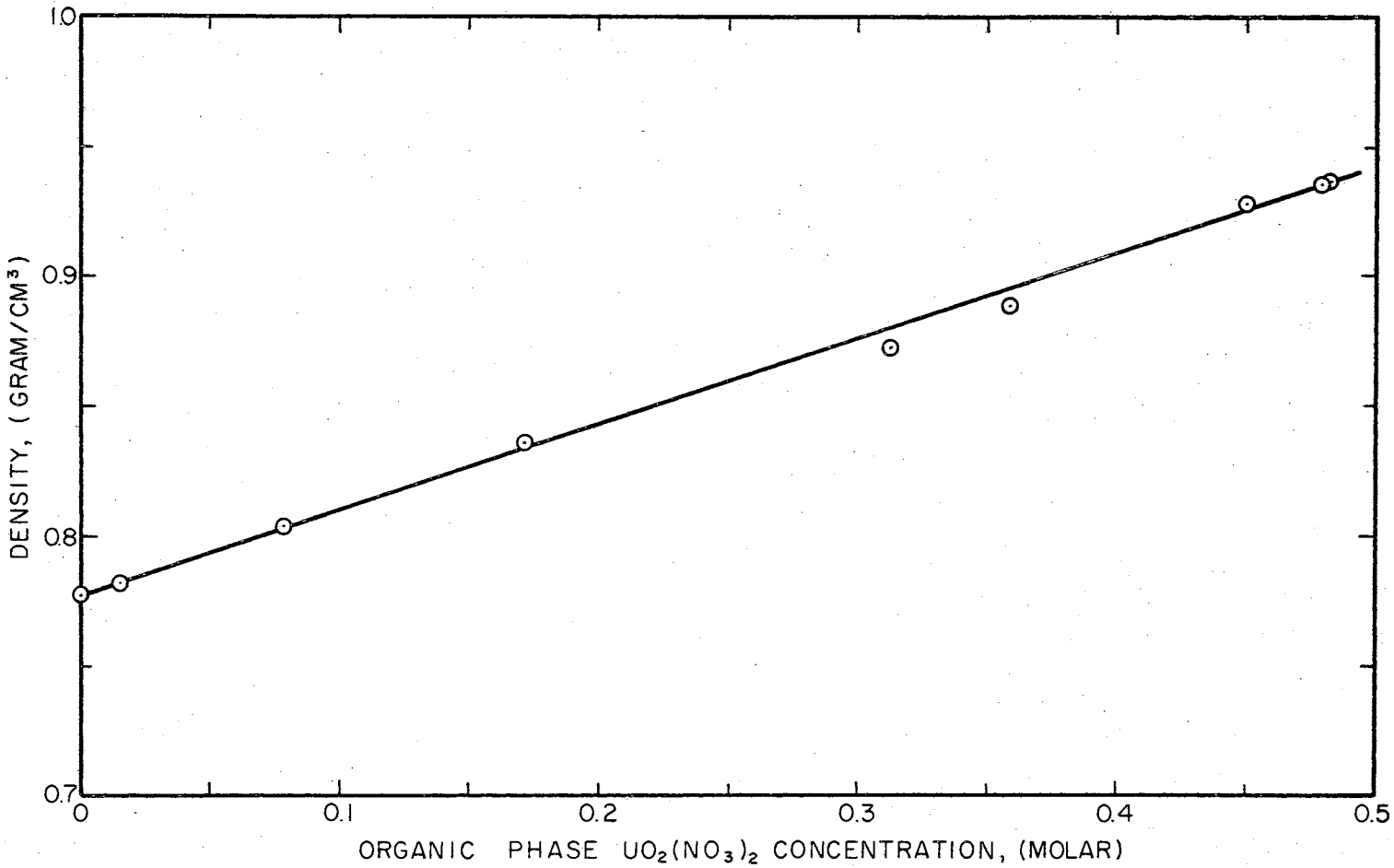

Figure 22. Density of TBP-n-Heptane-Uranyl Nitrate Solutions

using pycnometers. The average deviation of the density was found to be ± 0.00024 g/cm.^{3}.

Diffusivity

The diffusivity of the aqueous phase as a function of the uranyl nitrate concentration is obtained from the following equation derived from Finley (11):

$$D = 8.7379 \times 10^{-6} - 24.463 \times 10^{-6}\, C^{0.5} + 39.566 \times 10^{-6}\, C^{1.0} - 17.857 \times 10^{-6}\, C^{2.0} + 3.355 \times 10^{-6}\, C^{3.0} \qquad \text{(E-4)}$$

An average value of 1.86×10^{-6} was taken as the diffusivity of the organic phase for all concentrations. This value was arrived at from data collected by Finley where the organic phase was 70 percent Amsco and 30 percent TBP.

A P P E N D I X F

APPENDIX F

EXPERIMENTAL DATA

TABLE VII

TOLUENE-ACETONE-WATER SYSTEM

Run No.	Organic Phase Conc. Acetone in Equilibrium With Aqueous Phase Vol. %	Aqueous Phase Conc. Acetone in Equilibrium With Organic Phase Vol. %	Organic Phase Conc. Acetone From Which Solute is Transferred Vol. %	System Experiencing Interfacial Turbulence
46	0.0	0.0	5.0	Yes
47	0.0	0.0	3.0	Yes
48	0.0	0.0	1.0	Yes
49	0.0	0.0	0.5	No
50	45.2*	38.3*	47.2	Yes
51	45.2*	38.3*	46.2	Yes

* The solutions within the cell chamber were cloudy during the run.

TABLE VIII

TRIBUTYL PHOSPHATE-n-HEPTANE-URANYL

NITRATE-WATER SYSTEM

Run No.	Aqueous Phase Conc. $UO_2(NO_3)_2$ in Equilibrium With Organic Phase Molar	Organic Phase Conc. $UO_2(NO_3)_2$ in Equilibrium With Aqueous Phase Molar	Aqueous Phase Conc. $UO_2(NO_3)_2$ From Which Solute is Transferred Molar	System Experiencing Interfacial Turbulence
12	0.000	0.000	1.008	Yes
16	0.000	0.000	0.727	Yes
17	0.000	0.000	0.4975	Yes
18	0.000	0.000	0.423	Yes
19	0.000	0.000	0.3494	Yes
20	0.000	0.000	0.1699	Yes
21	0.000	0.000	0.113	Yes
22	0.000	0.000	0.05012	No
23	0.000	0.000	0.08971	Yes
24	0.000	0.000	0.07008	No
25	0.2037	0.1874	0.2999	Yes
26	0.2037	0.1874	0.2614	No
27	0.2037	0.1874	0.2837	Yes
28	0.2037	0.1874	0.2615	Yes
29	0.2037	0.1874	0.2422	No
30	0.7700	0.4260	0.9466	No
31	0.7700	0.4260	1.1065	Yes
32	0.7700	0.4260	1.0270	Yes
33	0.5472	0.3578	0.6017	No
34	0.5472	0.3578	0.6197	Yes
35	0.5472	0.3578	0.6013	No
36	0.5472	0.3578	0.6198	Yes
37	0.3754	0.3210	0.4141	No
38	0.3754	0.3210	0.4341	Yes
39	0.3754	0.3210	0.4141	No
40	0.3754	0.3210	0.4342	Yes
41	0.3754	0.3210	0.4243	Yes
42	0.0997	0.0597	0.1724	Yes
43	0.0997	0.0597	0.1407	Yes
44	0.0977	0.0597	0.1206	No
45	0.0997	0.0597	0.1311	Yes

A P P E N D I X G

APPENDIX G

COMPUTER PROGRAM FOR CALCULATING DISTURBANCE FACTOR

A modification of the computer program obtained from Marsh, Sleicher, and Heideger (22) is presented as a printout of the object deck. The data input was changed so that experimental values for the systems physical properties could be read into the program in place of the hypothetical values built into the program. This program was used to solve Equation G-1 using the 7040 IBM computer.

$$\frac{\mu_a}{C^\circ\ \zeta_a\ \alpha}\,\beta = \frac{\mu_a}{C^\circ\ \zeta_a\ \alpha}\,(\hat{\beta} + i\tilde{\beta}) = \frac{\frac{2m}{\sqrt{\pi}}\left[\left((q_b - 1)/(q_b - p_b)\right)\frac{1}{r} - \left((q_a - 1)/(q_a - p_a)\right)\right]}{\left[1 + p_a + (\mu_b)/(\mu_a)\ (1 + p_b)\right]\left[\frac{m}{r^2}\,q_b + q_a\right]\left[r + m\right]} \qquad \text{(G-1)}$$

The program determines a wave number that will produce the maximum disturbance factor for a given system. The real value $\hat{\beta}$ (disturbance factor) and the imaginary value $\tilde{\beta}$ of the growth constant β are calculated from the following physical properties of each phase of the system: (1) solute diffusivity, (2) absolute viscosity, (3) kinematic viscosity, (4) solute distribution coefficient, and (5) coefficient of interfacial tension. Comment statements are printed throughout the object deck to identify the symbols used in the program and to facilitate the use of the program.

The surface viscosity term in Equation 1, Chapter II, was deleted from the computer program. Also, Marsh, Sleicher, and Heideger replaced $(q_b - p_b)$ with $(q_b + p_b)$ and $(q_a - p_a)$ with $(q_a + p_a)$ in programming Equation G-1. They gave no explanation for the sign changes, so it was assumed that an error had been made in programming Equation G-1. However, when the signs were changed in the programs to the signs given in Equation G-1, the program would not converge to give an answer; so in this study the program was used without correcting the sign changes.

```
C      THIS PROGRAM CALCULATES THE DOMINANT OSCILLATORY
C      DISTURBANCE FOR A GIVEN SET OF PHYSICAL
C      PARAMETERS
C      IT IS NOW SET UP FOR LIQUID'LIQUID SYSTEMS
C      VISC IS THE ABSOLUTE VISCOSITY
C      E IS THE KINEMATIC VISCOSITY RATIO
C      VISK IS THE KINEMATIC VISCOSITY
C      EA IS THE ABSOLUTE VISCOSITY RATIO
C      ABC IS THE DIFFUSIVITY RATIO
C      CAB IS THE DISTRIBUTION COEFFICIENT
C      CON IS THE CONCENTRATION
C      BST IS THE INTERFACIAL TENSION GRADIENT
C      BAC IS THE DIFFUSIVITY
       WRITE (6,2)
     2 FORMAT(1H1)
     1 READ(5,7)VISC,E,VISK,EA,BAC
     7 FORMAT(5F14.8)
       READ(5,135)ABC,CAB,CON,BST
   135 FORMAT(4F10.5)
       PI = 3.14159
       VIS = 1.0/EA
C      AQ EQUALS CONC AND INTERFACIAL TENSION GRADIENT / VISC
       WRITE(6,8) VISC, E
     8 FORMAT(1H0// 5X, 20HVISCOSITY IN PHASE A, F20.5, 5X,
      1 15HVISCOSITY RATIO, F20.5,// 4X, 1HN, 1X, 2HNB, 1X, 2HNB, 2X,
      2 1HK, 1X, 2HNC, 4X, 9HZETA REAL, 4X, 9HBETA REAL, 8X, 5HALPHA,
      3 4X, 9HBETA IMAG, 9X, 4HBALP, 8X, 5HBNALP, 12X, 1HA, 4X,
      4 9HZETA IMAG)
       COMPLEX QA, QB, PA, PB, BAE, BAD, BA, DAE, DAD, DA, B, BD, Z
       DIMENSION QA(100), QB(100), PA(100), PB(100), BAE(100), BAD(100),
      1 BA(100), DAE(100), DA(100), B(100), BD(100), Z(100), ZETR(100),
      2 ZETI(100), BALI(100), BALR(100), ALPHA(100), BETAR(100),
      3 BETAI(100), TR(100), DAD(100)
       DIMENSION ZR(50), BETA(50), ALPA(50), BETI(50), BALP(50),
      1 BNALP(50), A(50), ZETIM(50)
C  DADB IS THE DIFFUSIVITY RATIO
       DADB=ABC
C  DIF IS THE DIFFUSIVITY
       DIF=BAC
C  DIST IS THE DISTRIBUTION COEFFICIENT
       DIST=CAB
       DIV=DIF
       EK=DIST
       R = DADB
       AQ=(CON*BST)/(VISC)
       D = DIV/VISK
       BB = 2.0*EK/((SQRT(PI))*(SQRT(R) + EK))
       BETR = 0.0
       ZD = 0.0
       ZR(1) = 0.5
C  METHOD OF GOLDEN SECTIONS TO FIND MAXIMUM AMPLICATION
C  FACTOR FOR OSCILLATORY DISTURBANCE
       DO 100 N = 1, 30
       NC = N
       Q = ZR(N)
C   Q IS THE REAL PART OF ZETA
       ZETI(1) = 3.4
       Z(1) = CMPLX(Q, ZETI(1))
C  TRIAL AND ERROR TO FIND ZETA IMAGINARY
       DO 30 I = 1, 99
       QA(I) = CSQRT( 1.0 + Z(I))
       QB(I) = CSQRT( 1.0 + R*Z(I))
```

```
      PA(I) = CSQRT( 1.0 + D*Z(I))
      PB(I) = CSQRT( 1.0 + D*E*Z(I))
      BAE(I) = (QB(I) -1.0)/((SQRT(R))*(QB(I)+PB(I)))
      BAD(I)=(QA(I)-1.0)/(QA(I)+PA(I))
      BA(I)=BAE(I)-BAD(I)
      DAE(I)=1.0+PA(I)+VIS*(1.0+PB(I))
      DAD(I)=(EK/R)*QB(I)+QA(I)
      4 '9'=4 5'9''4 4'9'
       (I)=++*++(I)OD+(I)
      BD(I)=AQ*B(I)
      21LR(I)=REAL(BD(I))
C     BALR=BETA OVER ALPHA REAL, BD=BETA OVER ALPHA
C     BALI=IMAGINARY PART OF BETA OVER ALPHA
      BALI(I)=AIMAG(BD(I))
      ZETR(I)=REAL(Z(I))
C     ZETI=IMAGINARY PART OF ZETA, ZETR=REAL PART OF ZETA
      TR(I)=Q*BALI(I)/BALR(I)
      WR=(ZETI(I)-TR(I))/5.0
      ZETI(I+1)=ZETI(I)-WR
      ALPHA(I)=BALR(I)/(DIV*Q)
      Z(I+1)=CMPLX(Q, ZETI(I+1))
      BETAR(I)=ZETR(I)*DIV*(ALPHA(I)**2)
      BETAI(I) = ZETI(I) * DIV * (ALPHA(I)**2)
C     BETAI = IMAGINARY BETA,   BETAR = REAL BETA
      K = I
      ZAB = ABS(TR(I) - ZETI(I))
      W = ABS(0.001 * ZETI(I))
      IF(ZAB - W) 35, 35, 30
   30 CONTINUE
   35 BETA(N) = BETAR(K)
      ZETIM(N) = ZETI(K + 1) - (ZETI(K + 1) - ZETI(K)) /2.0
      ALPA(N) = ALPHA(K)
      BETI(N) = BETAI(K)
      BALP(N)=REAL(B(K))
      BNALP(N) = BALP(N) * ALPHA(K)
      A(N) = -( ALPHA(K)) * (VISC**2.0)
C  ALPA IS ALPHA
C  BETA IS BETA REAL
C  BETI IS BETA IMAGINARY
C  BALP IS B WITH ALPHA INCLUDED
C  BNALP IS B TIMES ALPHA
C  A IS A
      IF(ZD - 0.001) 36,36,50
   36 IF(N - 2)37,38,39
   37 ZR(2) = 1.0
      GO TO 100
   38 IF(BETA(N) - BETA(N - 1))43,41,41
   41 ZR(N + 1) = ZR(N) + 1.0
      GO TO 100
   39 IF(BETA(N) - BETA(N - 1)) 44,42,42
   42 ZR(N + 1) = ZR(N) + 1.0
      GO TO 100
   43 ZO = 0.0
      ZD=ZR(N)
      ZR(N+1)=0.618*ZD
      GO TO 100
   44 ZO=ZR(N-2)
      ZD=ZR(N)
      ZR(N+1)=0.618*ZD+0.382*ZO
      GO TO 100
   50 WAD=ABS(BETR)
      IF(WAD-0.0001)51,51,52
```

```
 51 BETR=BETA(N)
    ZER=ZR(N)
    ZR(N+1)=0.382*(ZD-ZO)+ZO
    GO TO 100
 52 IF(BETA(N)-BETR) 60,60,61
 61 IF(ZR(N)-ZER)65,65,55
 55 ZO=ZER
    ZR(N+1)=(ZD-ZO)*0.618+ZO
    ZER=ZR(N)
    BETR=BETA(N)
    GO TO 95
 65 ZD=ZER
    ZR(N+1)=-(ZD-ZO)*0.618+ZD
    ZER=ZR(N)
    BETR=BETA(N)
    GO TO 95
 60 IF(ZR(N)-ZER) 70,70,75
 70 ZO=ZR(N)
    ZR(N+1)=(ZD-ZO)*0.618+ZO
    GO TO 95
 75 ZD=ZR(N)
    ZR(N+1)=-(ZD-ZO)*0.618+ZD
    GO TO 95
 95 WAE=ABS(ZR(N)*0.001)
    IF(ABS(ZR(N+1)-ZR(N))-WAE) 105,105,100
100 CONTINUE
105 WRITE(6,4) L, NB, NA, K, NC, ZR(NC), BETA(NC), ALPA(NC), BETI(NC),
   1 BALP(NC), BNALP(NC), A(NC), ZETIM(NC)
  4 FORMAT(1H0, 2X, 5I3, 1P8E13.4)
    GO TO 1
    END
```

A P P E N D I X H

APPENDIX H

NOMENCLATURE

A - proportionality constant

B - dimensionless growth constant

C - solute concentration, molar

D - solute diffusion coefficient, $cm.^2/sec.$

e - $\sqrt{\nu_a/\nu_b}$

f - focal length of lens

g - acceleration of gravity

H - distance of fringe deflection on negative, due to concentration gradient in cell

h - thickness of fluid layer

i - $\sqrt{-1}$

I_L, I_D - image size and image distance from lens, respectively

j_o - rate of change with temperature of the time rate of heat loss per unit area from the upper surface

K - coefficient of thermometric conductivity

L - dimensionless constant introduced by Pearson, $j_o h/K$

M - Marangoni number, $(\sigma \zeta h^2)/(\rho \nu K)$

m - distribution coefficient = C_b/C_a at equilibrium

O_L, O_D - object size and object distance from lens, respectively

P - object distance from center of lens

p - $\sqrt{1 + \beta/\alpha^2 \nu}$

Q - image distance from center of lens

q - $\sqrt{1 + \beta/\alpha^2 D}$

R - Rayleigh number, - $(g \gamma \delta h^4)/(K\nu)$

r - $\sqrt{D_a/D_b}$

t - time from start of diffusion run, sec.

X - spatial coordinate, vertical distance in cell

Z - spatial coordinate

Greek Symbols

α - wave number, 1/cm.

β - growth constant (a complex number), 1/sec.

$\hat{\beta}_o$ - amplification factor for the disturbance (real value of growth constant), 1/sec.

γ - coefficient of volume expansion

δ - rate of increase in temperature upward

ζ - concentration coefficient of interfacial tension, dynes/cm.-molar

μ - ordinary viscosity, g/cm.-sec.

μ_s - composite surface viscosity, g/cm.-sec.

ν - coefficient of kinematic viscosity, $cm.^2/sec.$

ρ - density of fluid, $g/cm.^3$

σ - rate of change of surface tension with temperature

Subscripts

a - phase A, phase from which solute is transferred

b - phase B, phase into which solute is transferred

c - critical value

o - initial condition

s - organic phase of $UO_2(NO_3)_2$ solution

w - aqueous phase of $UO_2(NO_3)_2$ solution

Superscripts

$\hat{}$ - real value of a complex variable

$\tilde{}$ - imaginary value of a complex variable

' - time corrected diffusion coefficient

VITA

Richard Donald Skinner

Candidate for the Degree of

Doctor of Philosophy

Thesis: INITIATION OF INTERFACIAL TURBULENCE IN LIQUID-LIQUID SYSTEMS

Major Field: Chemical Engineering

Biographical:

Personal Data: Born in Greenwood, Arkansas, February 15, 1939, the son of Richard Lee and Georgia Kathleen Skinner; married Sandra Sue Hadwiger, August 18, 1963.

Education: Attended grade school in Greenwood, Arkansas; graduated from Greenwood High School in 1957; received the Bachelor of Science degree from the University of Arkansas, with a major in Chemical Engineering, in June, 1962; received the Master of Science degree from the Oklahoma State University, with a major in Chemical Engineering, in August, 1964; completed requirements for the Doctor of Philosophy degree in July, 1967.

Professional Experience: Employed by the Natural Gas Pipeline Company of America, Joliet, Illinois, during the summer of 1962; at present an engineer in the Research and Development Department of Phillips Petroleum Company, Bartlesville, Oklahoma; membership in scholarly or professional societies includes Sigma Tau, Omega Chi Epsilon, Sigma Xi, and the American Institute of Chemical Engineers.